The degassing behavior of volatile heavy metals in subaerially erupted magmas and their chemical diffusion in silicate melts

by

Angela D. Johnson

B.Sc. hon., University of Alberta, 2007

A Thesis Submitted in Partial Fulfillment of the Requirements
For the Degree of

MASTER OF SCIENCE

In the School of Earth and Ocean Science

The degassing behavior of volatile heavy metals in subaerially erupted magmas and their chemical diffusion in silicate melts

by

Angela D. Johnson

B.Sc. hon., University of Alberta, 2007

Supervisory Committee:

Dr. Dante Canil (School of Earth and Ocean Science)
Supervisor

Dr. Kevin Telmer (School of Earth and Ocean Science)
Departmental member

Dr. Jay Cullen (School of Earth and Ocean Science)
Departmental member

Dr. Irina Paci (Chemistry Department)
Outside member

ABSTRACT

Supervisory Committee
Dr. Dante Canil (School of Earth and Ocean Science)
Supervisor

Dr. Kevin Telmer (School of Earth and Ocean Science)
Departmental member

Dr. Jay Cullen (School of Earth and Ocean Science)
Departmental member

Dr. Irina Paci (Chemistry Department)
Outside member

Volatile heavy metals are liberated from magmas during eruptive and passively degassing volcanic activity. Volcanic emanations have been estimated to contribute 20-40% of volatile elements such as Bi, Pb, As or Sb, and up to 40-50 % of Cd and Hg annually (Nriagu, 1989). Some workers, however, believe these ranges are too high (Hinkley, 1999) or too low (Zreda-Gostynska and Kyle, 1997) leading to considerable differences in global inventory budgets of these metals and the degree to which they load the atmosphere. The objective of this work is to investigate the behavior of volatile heavy metals such as Au, Tl, As, Pb etc. in subaerially erupted magmas and experimentally in silicate melts. Analysis of natural pumice samples confirm the futile, sporadic nature of Hg and associated heavy metals, suggesting these metals are fully degassed prior to deposition. Diffusion experiments were conducted in natural basalt, dacite and synthetic rhyolite (Ab-Or-Qz minimum eutectic) over a range of temperatures (1200 – 1430 °C) at 0.1 MPa. Starting compositions were doped with a heavy metal cocktail (Bi, Pb, Tl, Au, Re, Sb, Sn, Cd, Mo, As, Cu) and loaded into open top Pt capsules. One set of experiments examined the effect of melt composition (polymerization) on element diffusion, and the second investigated the effects of ligands on diffusion by adding known concentrations of Cl and S. During experiments of varying duration, concentration gradients arose in the volatile trace metals due to their varying volatility, as measured (normal to the melt/gas interface) by laser ablation inductively coupled plasma mass spectrometry (LA-ICP-MS) in quenched glasses. Diffusion profiles followed an Arrhenius relationship from which diffusion coefficients (D) and activation energies (E_a) were obtained for Au, Tl, As, Cd, Re, Pb and Bi (in decreasing order of volatility). Results show Au and Tl are the most volatile in dacite and rhyolite yielding $\mathrm{Log}D^{\mathrm{Dac}}{}_{\mathrm{Au}} = -10.7 \pm 0.1$ m^2/s and $\mathrm{Log}D^{\mathrm{Dac}}{}_{\mathrm{Tl}} = -10.9 \pm 0.1$ m^2/s in dacite, and $\mathrm{Log}D^{\mathrm{Rhy}}{}_{\mathrm{Au}} = -10.9 \pm 0.1$ m^2/s and $\mathrm{Log}D^{\mathrm{Rhy}}{}_{\mathrm{Tl}} = -11.3 \pm 0.3$ m^2/s in rhyolite respectively. The D for Au could not be measured in basalt but Tl was the fastest diffusing species $\mathrm{Log}D^{\mathrm{Bas}}{}_{\mathrm{Tl}} = -10.8 \pm 0.2$ m^2/s. Ligands Cl and S were shown to increase the volatilities of all metals, with S having a more profound effect. Diffusivities were applied to a simple 1D bubble growth model (Smith 1955). Model results indicate diffusion coefficients play a major role in metal fractionation processes occurring at depths that ultimately dictate what metal ratios are measured at the surface of volcanoes.

TABLE OF CONTENTS

LIST OF TABLES

LIST OF FIGURES

LIST OF APPENDICES

ACKNOWLEDGEMENTS

I would first off like to thank my supervisor, Dr. Dante Canil, for giving me the opportunity to work with him. Dr. Canil is an inspiring wealth of knowledge, and I sincerely thank him for his open door policy, guidance, editing of this thesis, financial support and exposing me to experimental petrology.

I owe a huge thank you to Dr. Jody Spence (UVic), for LA-ICP-MS assistance. Thank you Jody for your help with rock digestions, ICP reduction, patience and attention to detail. Many thanks to Dr. Mati Raudsepp and Edith Czech for their help on the microprobe at UBC.

Sincere thanks to the great faculty, staff, grads and undergrads in the Earth and Ocean Sciences department who made these past two years memorable, fun and rewarding. Thank you Jason Mackenzie for paving the way for this work, Steven Fellows and fellow office mates in B310 who I feel fortunate to have gotten to know over the last two years.

I would love to thank my parents Joanne and Leonard Johnson, who are the two most wonderful people I know and have always supported me in my education pursuits.

Chapter 1
INTRODUCTION

Trace metals are continuously transported throughout the Earth system via a finite number of 'sources' and 'sinks'. A fundamental concern with trace metal budgets is that the number of sources (anthropogenic pollution, forest fires, volcanoes, geothermal emissions ore deposits, etc.) greatly exceed the number of sinks (foliage uptake, subduction zones). This leads to a loading effect as metals concentrate in the atmosphere, at the Earth's surface, or in the oceans. There is much attention on the loading effect of Hg, Cd, As and other metals in the atmosphere and surrounding volcanoes (due to the high toxicity and environmental impacts of such metals) for which volcanism has been sourced as the major natural contributor (e.g. Pyle & Mather, 2003; Nriagu & Becker, 2003; Gustin & Lindberg, 2000; Gustin et al., 2008, Signorelli, 1997). For this reason, it is important to quantify what governs the rate at which toxic trace metals are being transported from magma to the exosphere.

As magmas ascend and decompress, their volatile species, originally supersaturated and in equilibrium with the melt, begin to exsolve into a vapour phase and nucleate to form bubbles. Trace metals partition into the bubbles which grow and rise with decreasing confining magmatic pressure (Lyakhovsky et al., 1996) to coalesce. The resultant liberation of volatiles in passive quiescent or eruptive magmatic degassing from volcanoes, fumaroles and solfataras (Ferrara et al., 2000) is the main mechanism of metal emissions to the atmosphere. Characterization of this process is essential in understanding eruptive dynamics (Villemant, 1999), geochemical reservoir cycling and atmospheric loading effects.

Large scale volcanic eruptions such as Mt. Pinatubo, Philippines (1991), Mt. Tambora, Indonesia (1815) or massive flood basalts such as the Deccan Traps, India (~65 Mya), emit enough ash, CO_2, SO_2 and other toxic metals and gasses into the atmosphere to significantly alter global climate patterns and cause major implications for the biosphere (Self et al., 2008; Nriagu & Becker, 2003 and references therein). It has been suggested that volcanic emissions may account for up to 50% of naturally occurring Hg and Cd and up to 40% of As, Cr, Cu, Ni, Pb and Sb emitted into the atmosphere annually (Nriagu, 1989).

The most abundant volatiles in magmas are H_2O, CO_2, S (as SO_2 or H_2S) and Cl (as HCl) with a lesser but significant component being volatile trace metals (e.g. Hg, Pb, Cd, Tl etc.). Trace metal fluxes are generally estimated indirectly by normalizing to SO_2 concentrations in volcanic plumes. The sporadic unpredictable nature of volcanic activity and varying metal/SO_2 ratios has lead to great uncertainty in annual metal fluxes. For example, estimates of Hg/SO_2 molar ratios span four orders of magnitude: 10^{-3} to 10^{-7} (Ferrara et al., 2000 and references therein).

Monitoring and collection of volcanic gases began in the 1790s (Britannica encyclopedia). Noguchi and Kamiya (1963) were the first to directly correlate SO_2 emissions and volcanic activity at Mt. Unzen, Japan. They suggested that monitoring SO_2 emissions may be used as a tool to indicate impending volcanic activity. This phenomena has since been studied for several volcanoes by a number of workers (e.g. Aiuppa, 2004, 2007; Wardell et al., 2008; Hirabayshi et al., 1982; Taran et al., 2002; Ohba et al., 2008, etc.). Work in parallel has began to measure concomitant trace metal fluxes from volcanoes as well.

Recently, Mackenzie & Canil (2008) experimentally measured trace metal diffusivities and applied them to datasets of trace metal contents in volcanic gases collected over the duration of different volcanic eruptions. They proposed that metal ratios (e.g. Cd/Re) could be used as a precursor to volcanic eruptions. This idea is based on the assumption that different trace metals have varying diffusivity and partition behavior, leading to their fractionation from one another into the gas phase. The resultant changes in metal ratios during different phases of an eruption could possibly indicate the maturity level of the magma in the chamber or conduit undergoing degassing.

The goals of this thesis are two fold. The first, is to measure the Hg content (and other metals) of subaerially erupted magmas after a volcanic eruption. In my first chapter, "The behavior of Hg in subaerially erupted magmas" pumice bombs generated from the 2360 B.P. sub-Plinian style eruption of the now dormant Mt. Meager, BC, Canada, were sampled. Bomb metal profiles were measured (normal to outer crust) by a LUMEX Hg analyzer and inductively coupled plasma mass spectrometer (ICP-MS). Profiles were then compared to textural/coloration changes in the bombs in an attempt to constrain the behavioral parameters that govern the mobility, speciation and solubility of Hg initially after eruption (as it is quenched in pumice), and after deposition as it is subjected to weathering/alteration processes.

In my second chapter "Experimental investigation of the degassing behaviour of Hg via proxy heavy metals in natural and synthetic silicate melts", I examine the diffusivity of important trace metals Au, Tl, Bi, Pb, Cd, Re and As, some of which may be used as a proxy for Hg (ie. those that are beside Hg on the periodic table, or have high volatility), as a function of temperature and melt composition. Diffusion experiments

were performed in natural basalt, dacite and synthetic rhyolite at magmatic temperatures to simulate shallow magmatic degassing prior to eruption. Diffusion coefficients were calculated and applied to a simple 1D bubble growth model to simulate the effect od degassing on trace metal ratios (Smith, 1955).

In summary, this thesis aims to better understand the chemical behavior of Hg, Au, Tl, Pb and other trace metals, both in natural magmatic systems and experimentally constrained in the lab. Further investigation of the mobility of heavy metals in natural silicate melts by experiment, as well as continued real-time gas measurements are essential in the ongoing quest for a volcanic prediction tool. Perhaps volatile heavy metal fractionation occurring at depth, and subsequent volcanic gas metal ratios liberated by magmatic degassing may aid in understanding volcanic processes that dictate an eruption. Hopefully this work may contribute, in some regards, to the lucrative goal of one day being able to successfully forecast volcanic eruptions, as well as help better constrain the behavior/mobility of these trace metals in nature and their loading effects on the atmosphere and biosphere.

Chapter 2

The degassing behavior of Hg in subaerially erupted magmas

2.1. INTRODUCTION

Mercury is an important trace metal to study due to its harmful loading effect on the bio- and hydrosphere. Mercury is strongly enriched in volcanic emanations (along with a wealth of other trace metals), and it has been estimated that 40–50% of naturally emitted Hg is sourced from volcanic emanations (Nriagu, 1989). While volcanoes are only one natural source of Hg, violent volcanic eruptions have the potential to inject enough volatile Hg into the atmosphere to change the global and regional cycle of mercury for a few years (Nriagu & Becker, 2003).

The complex speciation and atmospheric chemistry of Hg make it more difficult to measure than some other trace metals (eg. As, Cd, Tl, etc.) leading to significant uncertainties in the global volcanic input to the exosphere (Aiuppa et al., 2007 and references therein). Even such basic parameters as the mercury residence time in the atmosphere are not currently agreed upon. Pyle & Mather (2003) suggest a long (~1 yr) atmospheric residence time, whereas Gustin et al. (2008) believe it is on the order of hours to weeks. These fundamental variations, combined with the unpredictability of volcanic activity lead to significant differences in mass balance calculations when studying the global Hg budget. For this reason, global estimates of the volcanogenic Hg flux span three orders of magnitude.

Varekamp & Buseck (1986) estimate > 800 t/year of Hg, whereas Ferrara et al. (2000) are conservative in their estimate of ~1 t/year. More recently Nriagu & Becker

(2003) using a larger database of volcanoes, reported a flux of 112 t/year, however, Pyle & Mather (2003) question this estimate and suggest the actual output is closer to ~700 t/year (closer to Varekamp & Buseck (1986)). According to Pyle & Mather (2003), the lower volcanic flux estimates are based on an inappropriate extrapolation of data from low-temperature degassing at non-eruptive volcanoes, to high-temperature emissions from active volcanoes.

Despite the growing number of measurements of Hg in magmatic systems, we have no fundamental background knowledge of how this element behaves in igneous systems, such as its mobility, speciation, and solubility. What governs the behavior of Hg? Is it temperature or fluid/melt composition dependant? Why are some magmas more Hg-rich than others? Is it a byproduct of scavenging the crust en route to the surface before eruption, or are Hg concentrations inherent to the original parent magma? If non-arc volcanoes typically degas more sulfur-rich magmas and emit relatively greater amounts of SO_2 for a given VEI (volcanic explosivity index) (Carroll & Holloway, 1994) do they emit more sulfur-complexed volatiles? Is there any correlation with more Hg being emitted in these scenarios? Answers to these questions are necessary, and an understanding and characterization of the behavior of Hg in volcanic systems is critical to understanding its global inventory and loading effects.

The aim of this study is to better understand the behavioral parameters that govern the mobility, speciation and transport of Hg in volcanic systems. To do this, I have measured Hg (and other heavy metal) profiles in pumice bombs from Mount Meager, BC, Canada. Pumice is formed as a result of bubble ascent (from volatile nucleation) in a magma, forming a 'froth' layer at the top of a magma chamber which is assumed to

represent the state of the magma directly prior to eruption (Sparks, 1978). I have measured metal profiles to see if there are any correlations with textural/colouration changes, or cooling history present in the bombs.

2.2. GEOLOGY AND SAMPLING METHODS

Mount Meager is a Quaternary stratovolcano with up to 2000 m of local relief (Friele, 2004) located 150 km NNW of Vancouver, BC, Canada (Fig. 2.1). The 60 – 80 m thick fallout pumice deposit that was sampled in this study is associated with recent volcanism in the Garibaldi volcanic belt, which is the northern extension of the Cascade magmatic arc of the western United States (Russell et al., 2007 and references therein). Specifically, this pumice fallout deposit is underlain and overlain by rock avalanche deposits that were generated from the 2360 B.P. sub-Plinian style eruption of Mount Meager (Russel et al., 2007). This unit is contained in the volcaniclastic rocks of the Pebble Creek Formation, which are rhyodacitic-dacitic in composition and include non-welded to densely welded block and ash flow deposits, lava domes, and out-burst flood (lahar) deposits (Michol et al., 2008).

Approximately twenty surficial pumice bombs were collected in August 2008 at the Great Pacific Pumice Mine on Mount Meager from different areas of the open pit mine. Some were collected directly from the mining face with the intent that they were not exposed to weathering and leaching as much as the others. Only fully intact bombs were selected and ranged in size from 10 – 40 cm in diameter. The range in sizes was to

examine any differences in bomb size to metal mobility (with smaller bombs assumed to have cooled and quenched faster).

The bombs are pumaceous glass with a bulk vesicularity of >50% (Rust et al., 1999), containing sporadic lithic clasts, a variety of xenocrysts (i.e. quartz, hornblende etc.) and have distinctive outer 'bread crust' textures. Bombs with different surface colouration were chosen (ranging from light grey-white to yellow-orange) to examine any differences or correlations between colour and Hg content perhaps due to oxidation between bombs.

When cut open, the bombs exhibit a distinctive concentric colouration that ranges from light pink in the center of the bomb fading into an orangey-yellow and finally into a light grey-white outer crust (Fig. 2.2). Bombs with an outer crust of orange-red have brighter/bolder colours (perhaps more oxidized?) of pink-red in the center and throughout the bomb.

Bombs were cored through the center using a 1 inch diameter diamond drill bit at the Pacific Geoscience Centre in Sidney, BC. Most bombs were cored through the entire bomb, and bombs larger than the drill bit length were cored twice at either end (or at some angle to first core) to ensure the entire bomb was sampled. Cores were photographed and sliced normal to their axes into 0.5 cm slices using a small diamond saw. Half of each slice was ground by hand into powdered form using a mortar and pestle in preparation for analysis.

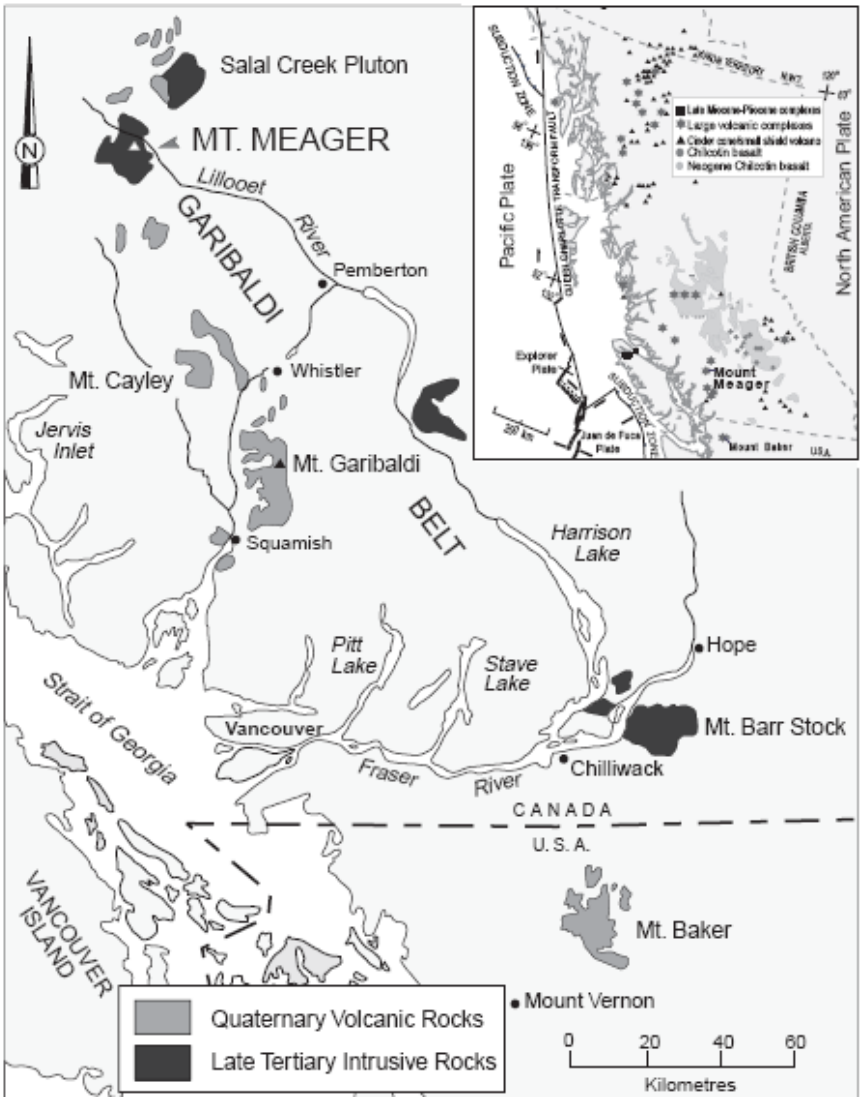

Figure 2.1. Geological Map of Mount Meager, BC, Canada. (Fig. 1 from Hickson et al., 1999).

2.3. ANALYTICAL METHODS

2.3.1. LUMEX RA-915+ Mercury Analyzer

A total of 12 sectioned bomb profiles (containing 13 – 15 0.5 cm ground slices) were analyzed in triplicates (~30 mg of sample per run) using the LUMEX RA-915+ Mercury Analyzer at the University of Victoria, BC. The LUMEX was operated in high-sensitive Air Mode (setting III) and utilized the Thermal Decomposition Zeeman corrected Atomic Absorption Spectrometry method (TDZ-AAS). The airflow pump was maintained at 5.5 L/min and PMT at 16,000 throughout analysis. The analyzer was calibrated at the start of every session with standards JGb-1 (gabbro, 4.78 ppb Hg) and JB-2 (basalt, 3.2 ppb Hg) with instrument drift corrected by resetting the zero baseline approximately every 10 minutes. Standards (JGb-1 or JB-2) were run between every six analysis to ensure accuracy throughout analysis. The detection limit was 0.2 ug/kg (0.2 ppb) (LUMEX operating manual).

2.3.2. Inductively coupled plasma-mass spectrometry (ICP-MS)

Core slices from three different bomb profiles (B4, B11, B14) were analyzed by inductively coupled plasma mass spectrometry (ICP-MS) X-Series II at the University of Victoria, BC, and a Perkin Elmer Elan 5000 ICP-MS at the University of Saskatchewan, SK. This work was done to compare Hg abundances with those of other trace metals. Ground 0.5 cm bomb slices (see methods) were digested separately with concentrated environmental grade HF and HNO_3 (Jenner, 1990; Longerich, 1990; Stefanova, 2003). Certified rock standards BCR-2 (basalt) and RGM-1 (rhyolite) were used for calibration to analyze the suite of trace metals Pb, Bi, Ni, Cu, Cd, Sn, Sb, Tl, Ir, Re, W and As.

Total procedural blanks (TPBs) and duplicates of 2 samples were run to ensure instrument precision and accuracy.

Data was reduced by hand from raw counts per seconds (CPS) to concentrations of ppm. The dilution factor (differences in mass of each sample) was corrected, data was normalized to the internal standard BCR-2 to account for primary drift, and secondary drift was corrected by normalizing to the element used for spiking samples (in this case Rh). Corrected CPS values were fit to a linear calibrated graph (CPS vs. BCR-2 concentrations) to obtain element concentrations in bomb profiles.

2.4. RESULTS

Mercury profile data from the LUMEX RA-915+ Mercury Analyzer selected from three representative Mt. Meager pumice bombs (M5, M9, M10) are shown in Figure 2.5 and summarized in Table 1. Most bomb profiles contained <1 ppb Hg and were right at or below detection limit for the LUMEX (0.2 ppb).

Even though the LUMEX was at or near its detection limit, the high sensitivity mode (Air Setting III) allowed for high quality accuracy in measurements which is evident from the standard deviations of triplicates analyzed (Table 1). Bombs M5, M9 and M10 were cored through the entire bomb (crust to crust) and were essentially Hg-free (<1 ppb) (Fig. 2.3). M9 and M10 had a slight increase in Hg (0.8 – 1 ppb) at one of the outer edges of the bombs, however, this increase was not fully matched on the opposite side and therefore was not a uniform characteristic. This increase was not inherent to all bombs, and others like M4 (Fig 2.4) exhibited rare sporadic increases in Hg in only one

or two slices that could not always be duplicated. M4A and M4B were cored from the same large (~22 cm) bomb at ~60 degrees to each other to see if they would produce similar Hg profiles.

Bomb slices were then analyzed for trace metals Pb, Bi, Ni, Cu, Cd, Sn, Sb, Tl, Ir, Re, V, Co, W and As by ICP-MS to examine if these metals correlated with any textural or colouration changes seen in the bombs. Inter-lab comparison between ICP-MS data from University of Victoria and University of Saskatchewan were in relatively close agreement, however, University of Victoria data was consistently 10 – 20% (or more) higher on all elements (Fig 2.5).

Trace metal profile data were visually compared to images of the bomb slices to see if colour or textural changes correlated with any of the elements listed above. No trends were observed. Ni in B4 (Fig. 2.6) slightly correlated with Hg, but Ni in the other bombs did not. Elements such as V, Ti, Zn, Fe, Ni, Co consistently correlated with *each other* but only slightly (and not always) correlated with Hg (Fig. 2.7). In Bomb 14, however, Hg anti-correlates well with metals V, Ti, Zn, Fe and Ni (Fig. 2.8). The other elements of interest were either below detection (As, Sb, Cd) or were in very low, sporadic concentrations (< 1 ppm) such as Pb, Ir, Bi, W, Sb, Sn, Re.

ICP analysis demonstrated the sporadic nature of the trace metals in subaerially erupted magmas and no correlation between colour or textural changes in the bombs and any metal could be established.

Figure 2.2. Mt. Meager core M5 (crust to crust) showing banding. All cores followed the same banding scheme: pink center followed by orange-red layer, yellow layer and white/grey outer 'breadcrust'.

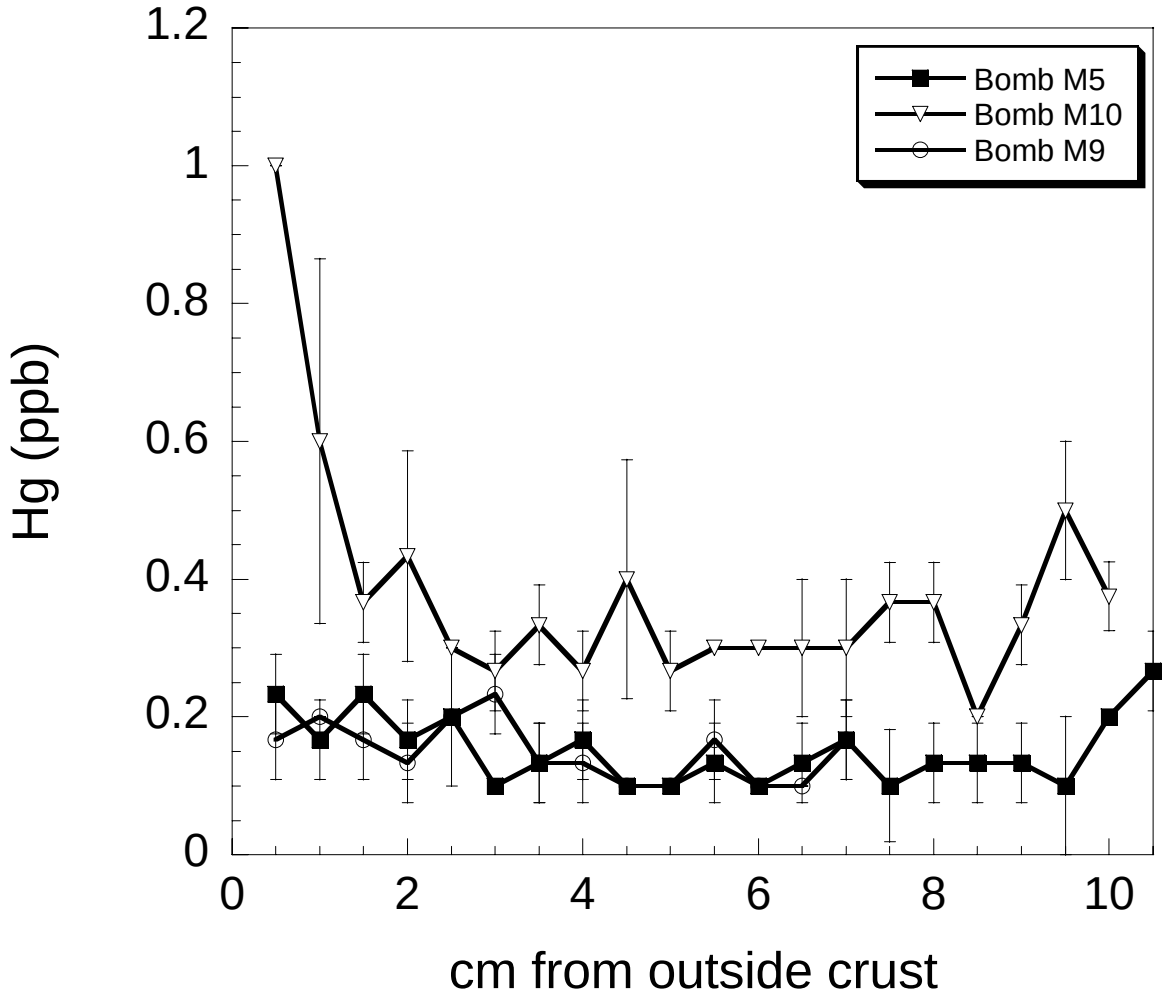

Figure 2.3. Mt. Meager pumice bomb profiles of bombs M5, M9, M10. Error bars are at 1σ standard deviation from triplicate analysis. Note: profiles show core through entire bomb (from crust to crust).

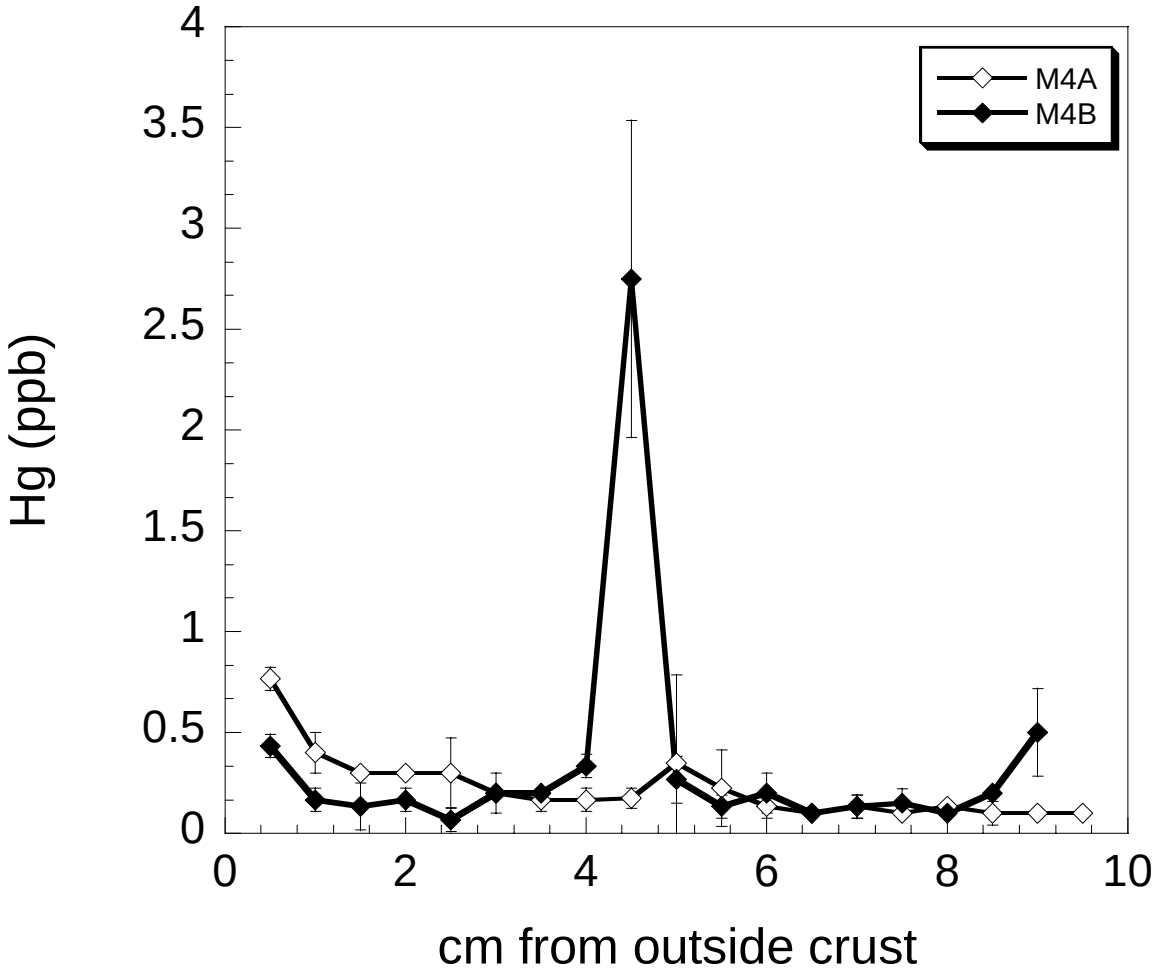

Figure 2.4. M4A and M4B cores from M4 bomb taken at ~60 degrees from each other. M4B shows Hg spike and M4A does not. Error bars are at 1σ standard deviation from triplicate analysis.

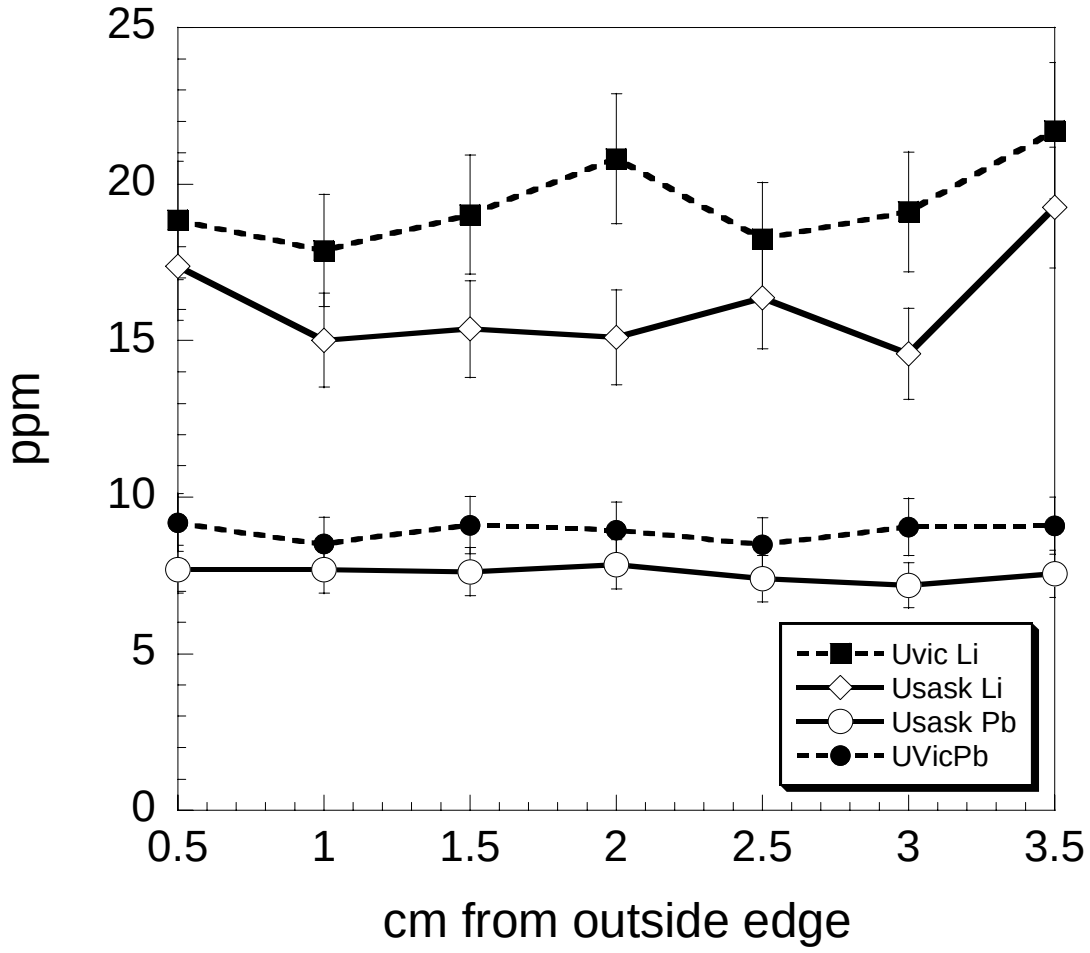

Figure 2.5. ICP-MS Inter-lab comparison for B11 between UVic and USask. Error bars are at 10%. UVic measurements were 10 – 20% higher than USask.

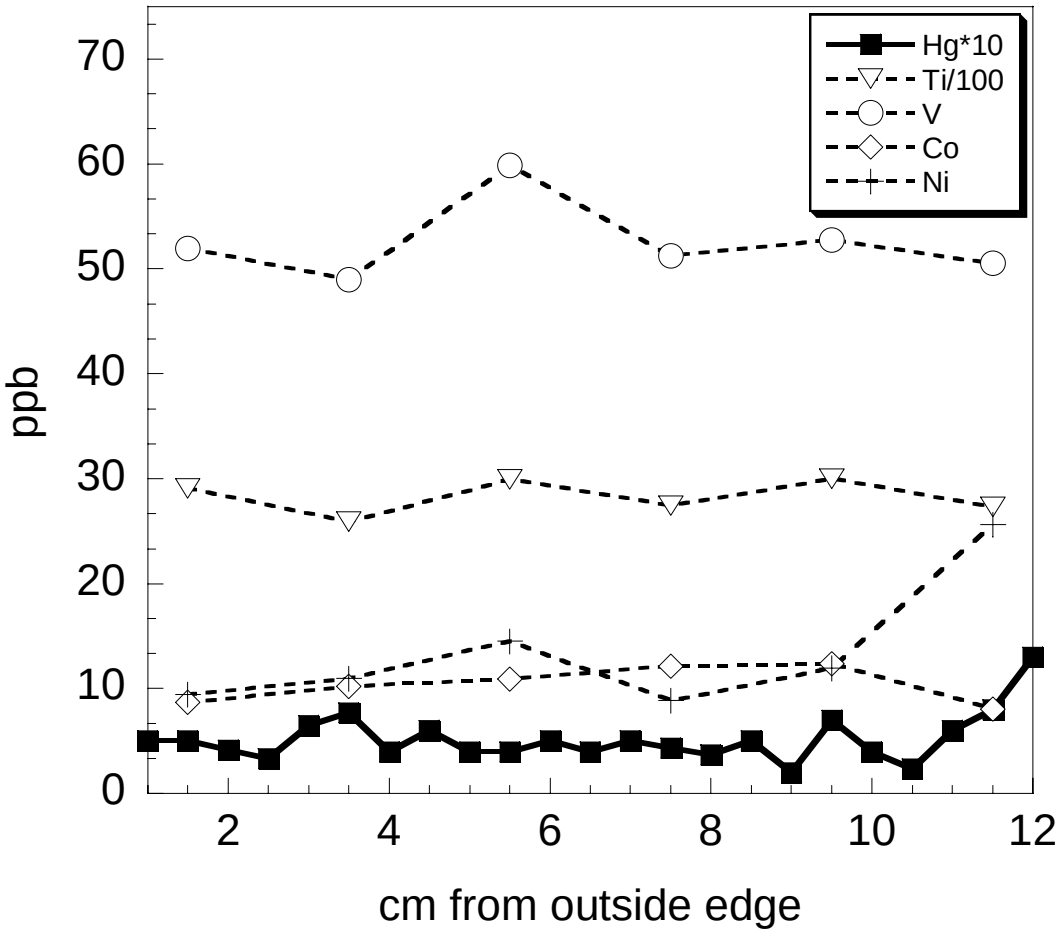

Figure 2.6. Bomb B4 shows slight correlation between Ni and Hg. Note: Hg in (ppb*10) for comparison, all elements in ppm.

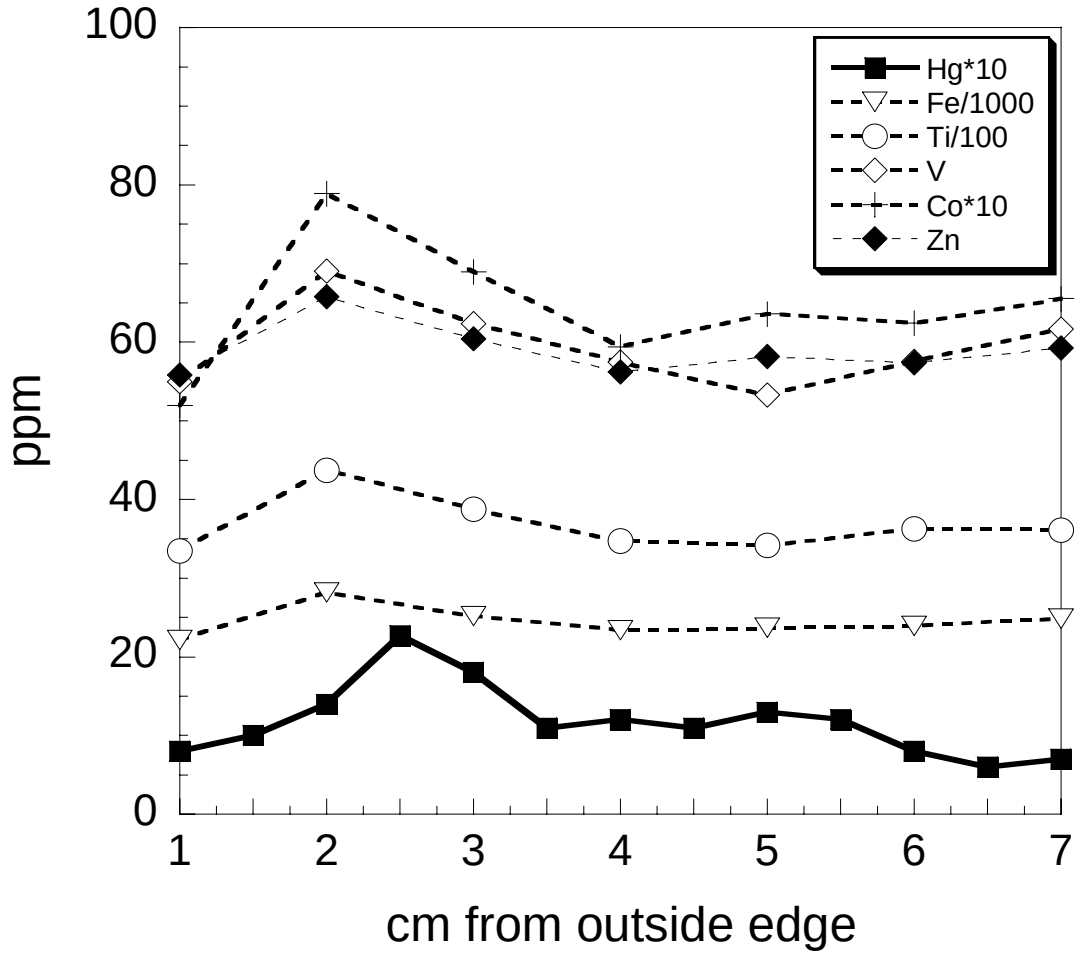

Figure 2.7. Bomb 11 V, Ti, Zn, Fe and Co correlate with each other, but do not significantly correlate with Hg. Note: Hg in (ppb*10) for comparison, all other elements in ppm.

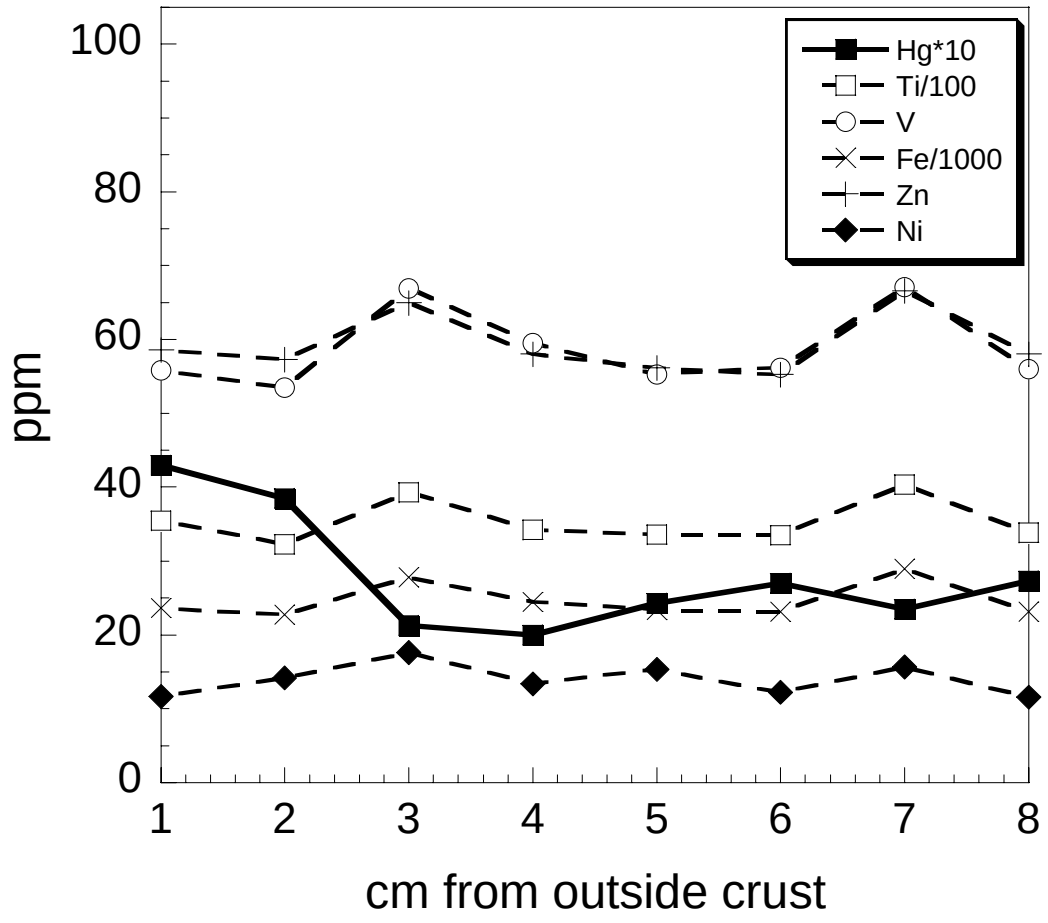

Figure 2.8. Bomb 14 V, Ti, Zn, Fe and Ni anti-correlate with Hg. Note: Hg in (ppb*10) for comparison, all other elements in ppm.

2.5. DISCUSSION

All the bombs analyzed (13 in total) had low, sporadic Hg and other trace metal concentrations that could not be correlated to any textural or colouration changes.

The random spike in Hg (Fig. 2.4) of core M4B and not M4A (from the same bomb) is not likely an accurate representation of Hg content concentrically throughout the bomb, and is probably the result of contamination or a small fragment of lithic clast that was not homogenized during powdering of sample.

I was not able to constrain the source of the pumice bomb colourations even after analyzing 13 heavy metals (Hg, Pb, Bi, Ni, Cu, Cd, Sn, Sb, Tl, Ir, Re, W and As). In any event, the colouration banding is an interesting phenomena that leaves questions and possible hypothesis as to its cause.

Initially, I set out to determine where the Hg consistently concentrates in the bombs: is it in sulphides, clays, glass or other xenocrysts or alteration minerals present? Alternatively, the banding could be a result of primary degassing of Hg (or other metal(s)) as it was quenched while being ejected into the atmosphere. Or was it simply a result of metal leaching or oxidation that happened after deposition as the bomb was subjected to over two thousand years of weathering and alteration? If the colour bands are in fact oxidation fronts of Hg or other metal(s), what controls this progressive rate of oxidation and does this change the speciation of Hg (from Hg^0 to Hg^{2+} to Hg_p)?

Ultimately there must be some metal(s) or mineral(s) responsible for the colouration banding of the pumice bombs, but this study failed to determine which they could be. The red-orange colouration would suggest iron oxidation plays a role, perhaps magnetite (Fe_3O_4) to hematite (Fe_2O_3), or oxyhydroxides such as goethite (FeOOH) or

ferrihydrite ($Fe_5HO_8 \cdot 4H_2O$) in the presence of water. It is also possible sulphides or sulphates cause the yellow-orange colouring band such as jarosite ($KFe_3(SO_4)_2(OH)_6$). CdS exhibits a bright yellow colour, or schwertmannite is an iron-oxyhydroxy-sulfate with a yellowish-orange colour, but typically precipitates in slightly acidic conditions (~3.2 pH). There are many minerals that share these colourings and these are just a couple possibilities.

The colour banding is uniform and if the bands are in fact a secondary leaching phenomena that occurred after deposition, it seems likely that leaching would be more dominant on top of the bomb and indicate a 'way up' or the direction from which the rain infiltrated into the deposit from the surface. This is not observed in any of the bombs in this study, or in any pumice bombs observed in the open pit mine which was visited on two separate occasions.

Perhaps the most important question when considering this colouration banding is - is this phenomena found in other fallout pumice deposits worldwide? And does the age of a deposit have any impact to pumice colouration or banding? For example, if this concentric banding is exhibited in older deposits and not younger ones, this would be evidence to suggest a secondary leaching/alteration origin. However, if younger deposits show this banding feature and older deposits do not, perhaps it is a primary degassing feature which is then leached away after being subjected to weathering. To my knowledge, there is no work on the causation behind these colouration bandings found in pumice bombs. There is a plethora of documented variable colourations of pumice ranging from white, grey, yellowish-white, pink, greenish-brown, brown or black (e.g.

Tait et al., 1998; Orsi et al., 1992; Paulik & Frank, 1997; Shane et al., 1998; Moriizumi & Nakashima, 2009; Cioni et al., 2003) but none on colouration banding.

Workers have attributed pumice colouration differences to iron oxidation (Fe^{2+}/Fe^{3+}) or primary banding of textural changes due to magma mixing (causing chemical/colouration changes that can be visually observed and analyzed). Pink, white and yellowish pumice units are reported in the Cretaio tephra in Italy (Orsi et al., 1992), however, the chemical data (major and minor elements) and isotopic data between these units are essentially identical and the cause for colouration difference was attributed to different eruption styles at different times.

Moriizumi & Nakashima (2009) experimentally measured color-change constraints in pumice in air by performing a series of heating experiments on them and measuring the experiments by spectrocolorimetry. They concluded their color changes were due to i) dehydration (causing yellowish colour) ii) oxidation to hematite or Fe^{3+} minerals forming (causing reddish colour) all controlled by diffusivity (D) of 1) water and 2) oxidation. This work is interesting because if this model is applied to Mt. Meager bombs then the outer yellowish band (underneath the grey-white 'bread crust') is a result of dehydration, the reddish layer below that to oxidation, and the pink center as the primary pumice colouration upon being quenched after eruption. This supports a primary degassing model controlled by diffusivity upon eruption.

2.6. SUMMARY

Mercury measurements in pumice bombs collected from Mt. Meager indicate virtually no Hg is present (< 1 ppb throughout) in bombs sampled. ICP-MS analysis show trace metals such as Ni, Cu, Pb, V, Ti, Co etc. are present but also exhibit sporadic, non-uniform behavior making them uncorrelatable with the concentric bomb colouration or textural changes.

The high volatility (or low boiling temperature) of Hg and some of the other trace metals analyzed (As, Bi, Cd etc.) makes these findings not surprising. This fallout pumice deposit was formed from a sub-Plinian style eruption, which produced an eruption column (of ejecta and gas) 14 – 18 km into the atmosphere (Russel et al., 2007). When considering the cataclysmic origin of this deposit, and the high surface area of the vesiculated glass in the pumice, it is no wonder that the most volatile metals (e.g. Hg, As, Cd etc.) were already degassed and those metals that were measurable (e.g. Ni, Cu, Co) exhibit no uniformity. It is possible this colouration banding phenomenon is a combination of all the processes discussed above: magmatic composition, primary degassing, secondary oxidation and/or leaching/alteration.

2.7. FUTURE WORK

Magnetic susceptibility (MS) measurements on the un-ground pumice slices could show correlation with alteration minerals or specific elements, since MS is a non-destructive method that is sensitive to mineralogy/alteration changes.

Sulfur was not analyzed. Total S would determine if yellow colourations correlated with sulphides or sulphates. Similarly Total Fe^{3+} could be measured or X-ray photoelectron spectroscopy (XPS) (which measures elemental composition and chemical state of a material) to determine if oxidation is responsible for the red-orange colour banding.

Table 1. LUMEX RA-915+ Hg data for pumice bombs M5, M9 and M10 from Mt. Meager.

Interval (cm)	M5 (ppb)	M10 (ppb)	M9 (ppb)
0.5	0.2	1.0	0.2
1.0	0.2	0.6 (0.3)	0.2
1.5	0.2	0.4	0.2
2.0	0.2	0.4 (0.2)	0.1
2.5	0.2	0.3	0.2 (0.1)
3.0	0.1	0.3	0.2
3.5	0.1	0.3	0.1
4.0	0.2	0.3	0.1
4.5	0.1	0.4 (0.2)	0.1
5.0	0.1	0.3	0.1
5.5	0.1	0.3	0.2
6.0	0.1	0.3	0.1
6.5	0.1	0.3 (0.1)	0.1
7.0	0.2	0.3 (0.1)	0.2
7.5	0.1	0.4	
8.0	0.1	0.4	
8.5	0.1	0.2	
9.0	0.1	0.3	
9.5	0.1 (0.1)	0.5 (0.1)	
10.0	0.2	0.4	
10.5	0.3		

Errors are <0.1 ppb (unless otherwise stated in brackets) standard deviations of triplicates analyzed.

CHAPTER 3

Experimental investigation of the degassing behaviour of volatile heavy metals in natural and synthetic silicate melts

3.1. INTRODUCTION

Magmas degas as the result of super saturation of volatile species, often in response to depressurization with ascent or crystallization (Carrol & Holloway, 1994). The degree to which elements partition into the gas phase is a function of element volatility, or its affinity for the vapor phase, equilibrium solubility, temperature, magmatic composition, and ascent rate, all of which are the main driving forces behind volcanic eruptions. Metals that partition from magma to the gaseous or particulate form are released in volcanic plumes, often complexed with halogens or sulfur. These plumes, are assumed to be the cooled, air-diluted equivalents of the high-temperature vapour phases originally in contact with melts, and transport a significant amount of trace metals from the mantle to the exosphere (Hinkley et al., 1994).

Measurements of volcanic gas compositions report an increase in S/Cl ratio directly before or during eruptions (e.g. Noguchi and Kamiya, 1963; Giggenbach, 1975; Menyailov, 1975; Menyailov et al., 1986; Hirabayashi et al., 1982; Crowe et al., 1987; Taran, 2002; Aiuppa, 2004; etc). Noguchi and Kamiya (1963) were some of the first authors to propose the possibility that certain ratios of aerosols or gas particulates emanating from a volcano may be useful in indicating impending volcanic activity, due to influxes of fresh, undegassed magma to the system. Recently, Aiuppa (2007) collected volcanic gas data from Mt. Etna, Italy, and showed a 50-fold increase in CO_2/SO_2 in the

days prior to eruption. Similarly, Ohba et al. (2008) directly correlated lava flux and SO_2 gas emissions at Mt. Unzen, Japan. These and other studies make it generally accepted, that monitoring volcanic gases could be a viable method of forecasting volcanic eruptions (Crowe et al., 1987).

Volcanoes are a significant natural source of toxic trace metals that impact the environment (e.g. Hg, Cd, Tl, Pb). There is an increasing interest to quantitatively confirm, as best as possible, the annual volcanic emissions or the rate at which they load the atmosphere. Improvements in remote sensing and analytical techniques have allowed for a growing number of volcanic gas measurements, specifically SO_2, which are readily monitored. Most metal fluxes are based on normalizing with reference to SO_2 which has allowed for a growing number of volatile trace metal *estimates* during pre-, syn- and post-eruption phases from volcanoes. However, due to the episodic nature of volcanic eruptions, and limited '*real-time*' data collected, it is not surprising that the rates at which metals, especially highly toxic ones, are degassed into the atmosphere vary by three orders of magnitude (Pyle & Mather, 2003).

Experimental data on the volatility of trace metals lag behind their measurement in volcanic eruptions. There is a considerable amount of experimental data on the volatility of metals from silicate liquids in the glass science literature, predominantly in borosilicate glass melts, or various alkali-lime silicate glass melts (e.g. Claussen & Russel, 1997; Clausen at al., 1999; Gerlach, 1998; von der Gonna, 2000). This data bears on the behaviour of polyvalent ions in the production of synthetic materials in windows, crystal growth or nuclear waste storage (Mungall & Dingwell, 1997 and references

therein). Most of these melts have no direct geological significance for the behaviour of trace metals in natural magmas at high temperatures.

This study investigates the degassing behaviour of heavy metals Au, Tl, Cd, Re, As, Pb and Bi from geologically relevant silicate liquids at 0.1 MPa between 1200 – 1430 °C. These metals were chosen on the basis that there is a dearth of information on their behaviour, and furthermore some of them may be used as a proxy for Hg, for which there is much attention on its loading effect in the atmosphere (Pyle & Mather, 2003; Nriagu & Becker, 2003; Gustin & Lindberg, 2000; Gustin et al., 2008 etc.). I report some of the first measurements of diffusivities for Au and other elements at these high temperatures in natural basalt, dacite and synthetic rhyolite for comparison. I apply the diffusivities in a simple 1-D bubble growth model to observe differences in metal ratios in gases that ultimately collect in volcanic plumes. My data and further knowledge of the kinetic and thermodynamic parameters controlling the behaviour of these metals may ultimately assist in forecasting volcanic eruptions.

3.2. EXPERIMENTAL METHODS

Elemental diffusion in silicate melts is a chemical process driven by chemical-potential gradients (Kretz, 1994). When an element is volatile from a silicate liquid, it migrates under a chemical flux across the gas/liquid interface, imposing a diffusion gradient dependent on element volatility (or affinity for the vapor phase), temperature, pressure and melt composition. The melt is contained in a Pt capsule that only allows for one dominant direction of diffusion (out the top). In this way, we aim to address how

temperature and melt composition affect element diffusion when pressure is held constant (0.1 MPa).

The experimental design differs from a natural magmatic system in a few different ways. Firstly, the experiments are conducted at constant pressure in small 3 mm diameter capsules, in which there is no flow or convection, and no changes in pressure, such as would occur during magma ascent and emplacement. Secondly, the experiments are performed in air, and trace metal complexes exist in a highly oxidized melt, lacking C-O-H fluids. Lastly, to avoid the presence of crystals, experiments are performed at super-liquidus temperatures above those of natural magmas.

To observe the effect of polymerization (silica content) on diffusivity I used three different starting compositions: 1) A natural pillow basalt from the Eocene Metchosin Igneous Complex, Vancouver Island, BC, Canada. 2) A natural dacite from the Quaternary pumice fall out deposit of Mt. Meager, BC, Canada and 3) a synthetic rhyolite melt at the Ab-Or-Qz minimum (Table 3.1). Natural starting materials (basalt and dacite) were prepared by crushing and grinding natural sample into powdered form under alcohol in an agate mortar with pestle and dried under a heat lamp for 30 minutes at about 150 °C. The dried powder was fused at 1300 °C overnight in a Pt crucible, quenched into a glass and powdered again.

Synthetic melt at the Ab-Or-Qz minimum eutectic was prepared by weighing out and mixing reagent grade 76.5% SiO_2, 9.8% Al_2O_3, 4.8% Na_2O, 4.9% K_2O and 1.8% $CaCO_3$ to make up an Ab-Or-Qz material of ratio 25-35-44 plus 1% Ca. The mixture was heated step-wise (800 °C for 1 hr, 900 °C for 1hr etc. until reaching 1500 °C) to

allow for decarbonization, fused overnight at 1500 °C, quenched to a glass, and then powdered similar to method above.

Approximately 5 g of each starting material powder was then doped using a micropipette with 2 mL of a prepared NIST certified standard solution in HNO_3 containing a heavy metal 'cocktail' of ~70 ppm of Au, Bi, Cd, Pb, Re, Sb, Sn, Mo, As, Cu, Tl using a micropipette. To ensure homogenization of elements added, the mixture was re-ground for 20 minutes under alcohol and dried under a heat lamp for 30 minutes. The powder was again fused at 1300 °C for 20 minutes, quenched and powdered. The second fusion was chosen to allow enough time for homogenization but was necessarily short so that highly volatile metals, such as Tl and Au, remain in the melt for subsequent diffusion experiments. Concentrations of heavy metals that remained in the melt prior to experimental runs are given in Table 3.2.

To compare the effects of Cl and S on diffusivity, two other basalt starting materials were made by the above methods with except approximately 5000 ppm Cl (as NaCl) was added to one, and 5000 ppm S (as $CaSO_4$) to the other. Typical Cl and S concentrations in arc-type basalts are 500 – 2000 ppm (Wallace, 2005), however, due to the high volatility of these elements, an unnatural amount was added to ensure Cl and S remained in the melt during fusion for experiments.

For each experiment, the starting powder was packed into a 2 mm or 3 mm O.D. (outer diameter) open ended Pt capsule, set in an alumina holder, and placed into a 'bucket' that hung from an alumina rod in the hotspot of a high temperature vertical tube furnace (Fig. 3.1). Temperature was measured using a Type B thermocouple that was directly adjacent to the sample and held constant to within ±1 °C. Experiments were run

at varying durations (5 min to 20 hr) and temperatures (1200 – 1430 °C). The melts were quenched to a glass within 30 seconds after the experiment by removal from the furnace and quenching in a stream of air.

Capsules were mounted lengthwise in epoxy, polished in half and then examined in reflective light to ensure no crystals or oxides were present.

3.3. ANALYTICAL METHODS

3.3.1. Electron Microprobe

Major and minor elements of starting materials and run products were analyzed by wavelength dispersive analysis using a CAMECA SX50 electron microprobe (EMP) at the University of British Columbia. A peak counting time of 30 s was used for all elements (Na, Mg, Al, Si, K, Cr, Ca, Ti, Mn, Fe, Cl) at 15 kV acceleration with a beam diameter of 10 um and a beam current of 20 nA. NIST standard 1520 was used as an external check before and after analysis. Line scans were carried out perpendicular to the melt/gas interface into the charge, and from the center of the charge to the Pt wall (Fig. 3.2). All major elements analyzed remained homogenous, and no compositional gradients of major elements including higher volatilizing elements such as Na were observed (Fig. 3.3).

3.3.2. Laser ablation-inductively coupled plasma-mass spectrometry (LA-ICP-MS)

Trace element analysis was performed at the University of Victoria using an New Wave 213 nm UV laser coupled to a Thermo-Instruments X-Series II ICP-MS. Line scans perpendicular to the melt/gas interface into the charge were carried out at a rate of 5

um/s, with a 40 um laser spot size and an energy of ~1.9 mJ. Data was collected for ~ 500 s with an allotted 20 s before and after sample analysis to measure background concentrations. A peak counting time of 10 ms at each element was used at a frequency of 20 Hz. NIST certified SRM (standard reference material) standards 615, 613 and 611 were used as standards with Ca^{43} as an internal standard. NIST standards were analyzed after every 5-6 charges to ensure accuracy. Line scans with the laser were also performed from the center of the charge to the wall of the Pt capsule to observe if any metals were lost to the Pt. Data was collected and averaged over 2 s scan slices, and reduced from raw counts per second (CPS) to ppm using the Thermo© data reduction software.

3.4. DATA REDUCTION

I make two assumptions in this study of diffusivity. First, I treat the Pt capsule and melt as a one-dimensional semi-infinite medium, and assume that the flux of any species is out the top, into air. While some elements may diffuse into the Pt at longer runs, the experiments were performed at shorter intervals, and it is shown by subsequent analysis that diffusion driven by volatility out the top of the Pt capsule is the dominant loss process. The second important assumption is that I have created a static melt/gas interface where convection in the melt is negligible. While this is physically impossible to prove, the observation of smooth chemical gradients would infer that convection has not occurred, as movement in the melt would ultimately interfere with the diffusion profiles observed (Fig 3.3).

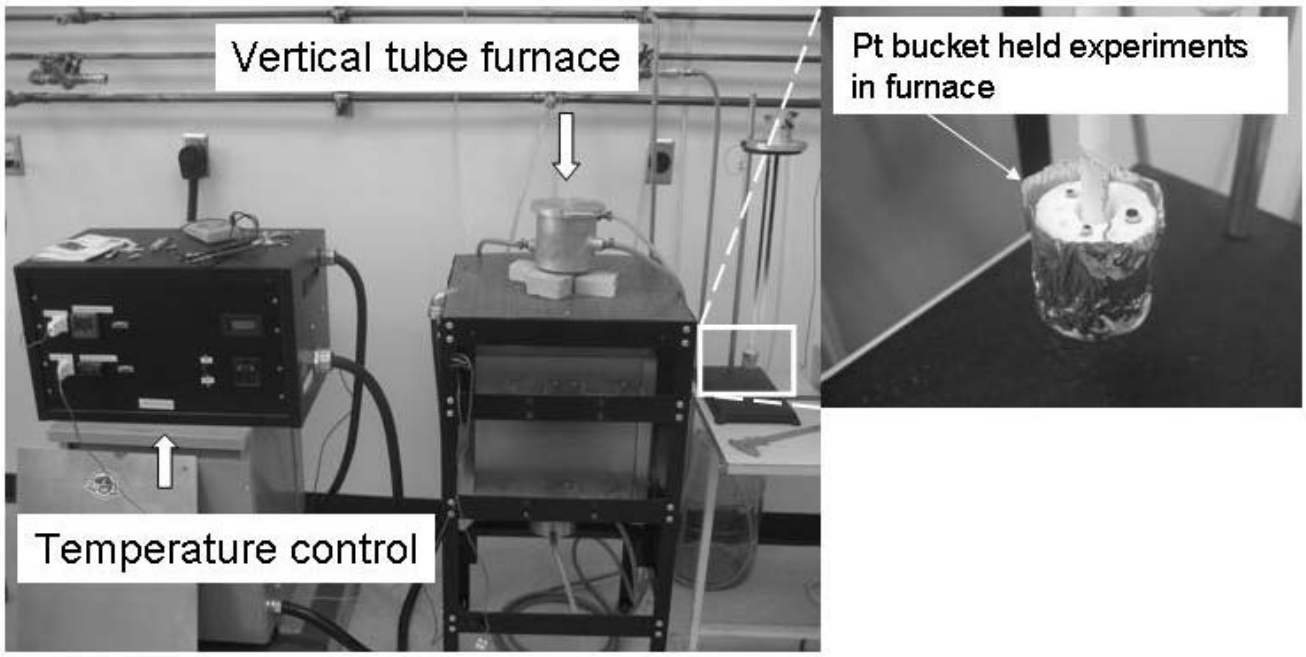

Figure 3.1. Set up for vertical tube furnace experiments.

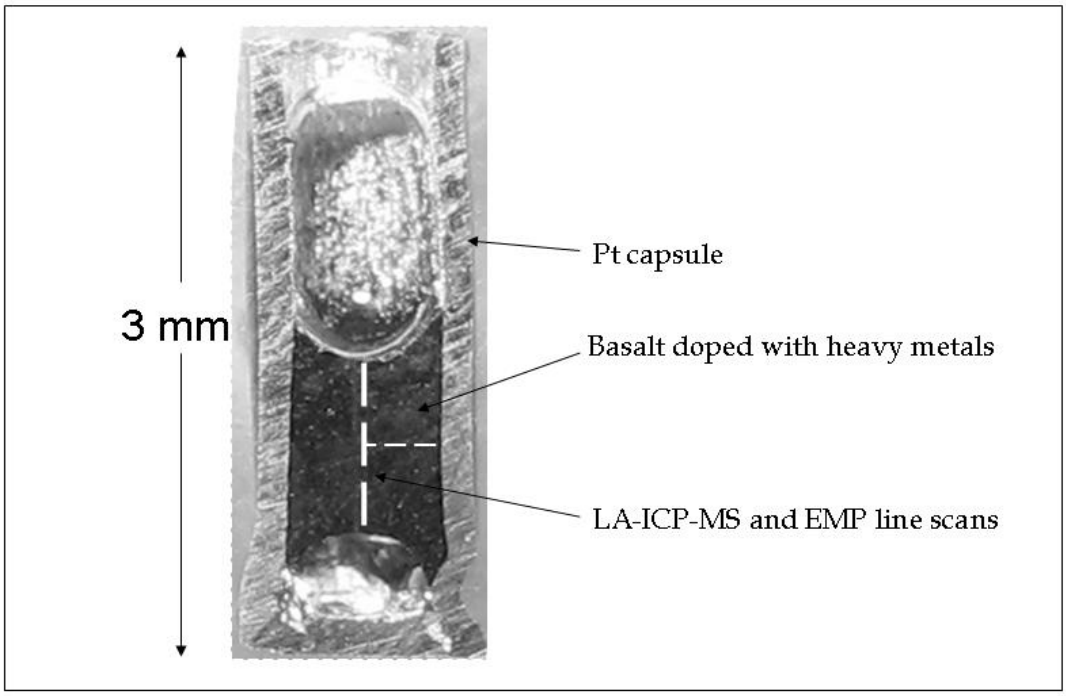

Figure 3.2. Experimental charge of 3 mm O.D. (outer diameter) Pt capsule with 'metal doped' basalt. LA-ICP-MS and electron microprobe (EMP) line scans are dashed lines.

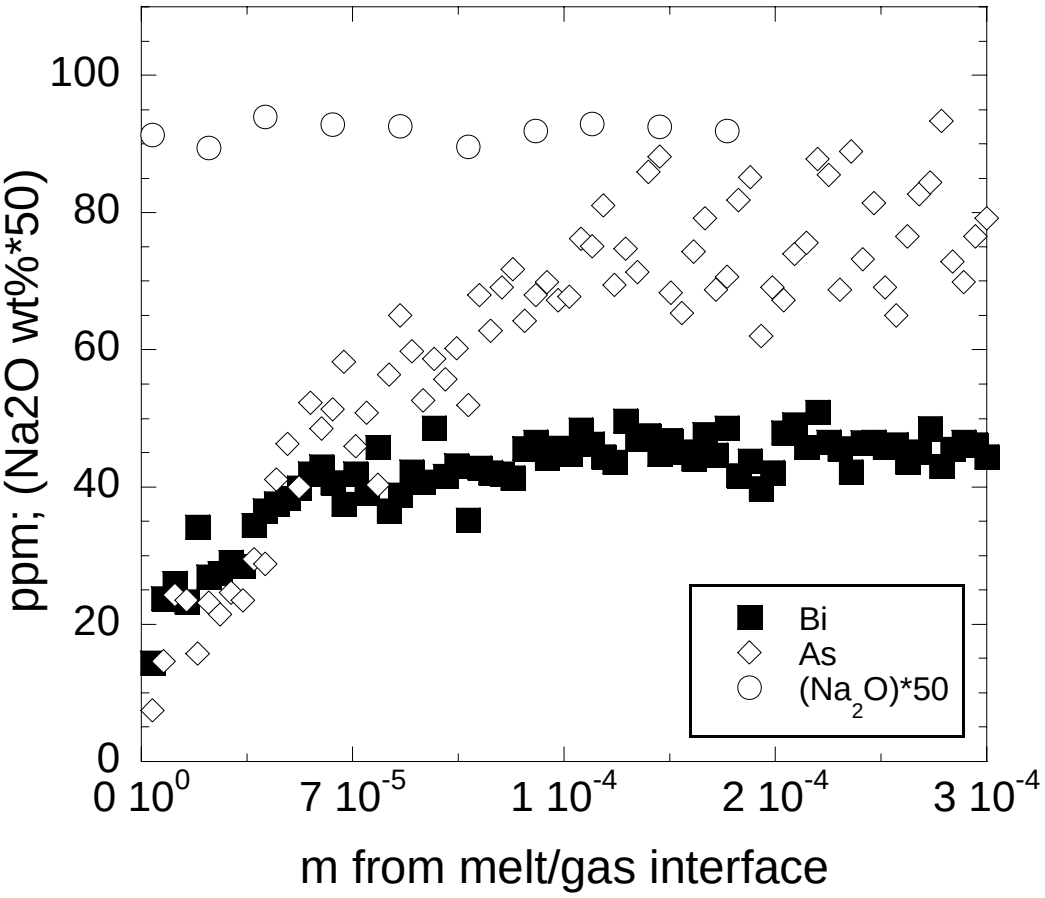

Figure 3.3. LA-ICP-MS and EMP line scans of Bi and As (in ppm) and Na_2O (in wt% multiplied by 50 for comparison) in a basalt experiment run at 1400 °C for 15 minutes. Line scans are from the melt/gas interface into the charge (glass). Each point is an average of 1s (5um) time slice of line scans. Bi and As show element diffusion profiles whereas Na_2O remains constant.

With these assumptions in place, I assume that any chemical gradient at any given distance *x* from the interface in the charge is a function of the chemical gradient potential created at the melt/gas interface according to Fick's 1st Law:

$$J = -D\ dc/dx \qquad (3.1)$$

where there diffusion coefficient (*D*) is the constant of proportionality between the flux of material or diffusing species (*J*) and the chemical concentration gradient or "driving force" (*dc/dx*) normal to the plane which is the fundamental basis for solving all diffusion problems (Freer, 1981). In my experiments, different trace element concentration gradients arise for different trace metals in the melt due to their varying volatility. I apply Crank's relationship of diffusion in a one-dimensional semi-infinite medium to extract diffusion coefficients (*D*):

$$x/ (2\sqrt{Dt}) = erf^{-1} (C - C_s/C_o - C_s) \qquad (3.2)$$

where erf^{-1} is the inverse error function, *C* is the concentration at distance (x), C_o is the initial concentration and C_s is the concentration at the surface. The compositional gradient, or driving force required for diffusion is the 'change in concentration term' (C-$Cs/C_o - C_s$). Ideally, when $erf^{-1}(C - C_s/C_o - C_s)$ is plotted against distance (*x*) from the melt/gas interface, a straight line with a slope equal to $1/2\sqrt{D}t$ is produced in which the diffusion coefficient (*D*) can then be derived (Crank, 1975).

A series of experiments over a range of temperatures then allows an estimate of the activation energy for diffusion (E_a) and its temperature dependence is described by the Arrhenius equation:

$$\log D = \log D_o - E_a/2.30RT \qquad (3.3)$$

where D is the diffusivity at temperature T (K), D_o is the pre-exponential or frequency factor, and R is the gas constant. Plots of log$D$ versus $1/T$ yield straight lines in which E_a can be extracted and extrapolated to conditions outside those of the experiments (since E_a and D_o are constant over a wide range of temperatures). The Arrhenius relationship is derived from the absolute rate theory which states that ions diffuse in discrete jumps. The energy barrier that must be reached in order for this to happen is the activation energy of diffusion (*Ea*) (Glasstone et al., 1941). D_o is related to the frequency at which this occurs, hence the name frequency factor. D_o is weakly dependent on temperature and is generally accepted as a constant (Mungall et al., 1999 and references therein).

3.5. RESULTS

3.5.1. Reproducibility of Experiments

The reproducibility of experimental diffusion coefficients from this study can be assessed in four ways. To ensure diffusion was not dependent on time, experiments were run at varying durations (5 min – 20 hours) at constant temperatures, similar to Chakraborty et al. (1995), Mungall (1997), and Dingwell & Scarfe (1985). I found that in extremely long run durations (>10 hrs) diffusion coefficients were smaller at the same temperature. For example, As in basalt at 1300 °C yielded Log^{Bas}_{As} = -11.87 m^2/s and -11.90 m^2/s at 2 and 4 hours respectively, whereas at 6 hours Log^{Bas}_{As} = -12.92 m^2/s. This is apparent in some other elements in other compositions. Therefore, I only used shorter experiments to ensure diffusion was only dependent on temperature and not time. Longer duration run data were only used if a shorter run time produced the same D (all run data

in Table 3.4). Secondly, I ran identical experiments at the same time (i.e. two separate basalt charges at 1400 °C 15 minutes during the same run.) as well as on different days to check consistency of results. Thirdly, to ensure diffusion was occurring perpendicular to the melt/gas interface (and convection was not occurring) I ran three line scans parallel to each other (perpendicular to the melt/gas interface through the entire charge) in several charges and observed no difference in chemical gradients. Lastly, I ran LA-ICP-MS line scans from the melt/gas interface into the charge (glass), and in the opposite direction from the charge to the melt/gas interface to ensure both element profiles were similar, and that memory effects in the ICP were not effecting diffusion profiles observed. Rare earth elements (RRE) Sm and Yb were also analyzed in LA-ICP-MS line scans to ensure diffusion was only occurring for volatile elements; these immobile REE remained constant.

To ensure diffusion was dominantly occurring out the top of the capsule, and that there was no or minimal loss of metals to the Pt wall capsule, LA-ICP-MS line scans were run towards the Pt capsule walls (Fig. 3.1). Some elements (Bi, Sn, Sb) can clearly be shown to be diffusing into the Pt, but this was only evident in higher temperature and longer duration experiments (e.g. 1400 - 1430 °C, > 4 hr). Loss of these elements into Pt was orders of magnitude smaller than their diffusion out the top of the capsule (Fig. 3.4).

3.5.2. Diffusion Coefficients and Activation Energies

I use the inverse error function to extract diffusion coefficients for each element (Fig. 3.5). Calculated diffusion coefficients at 1260 °C and activation energies (E_a) from experimental runs are summarized in Table 3.3 for elements that produced diffusion

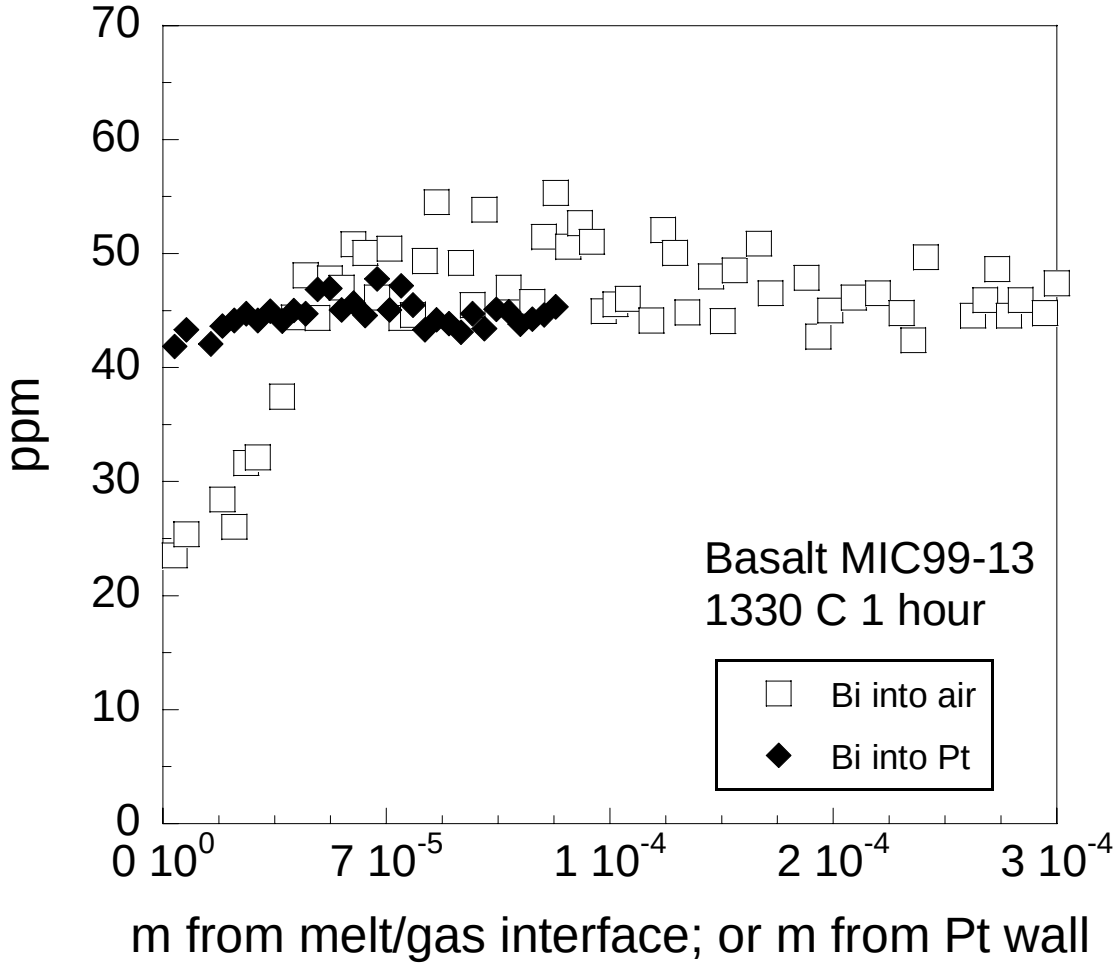

Figure 3.4. LA-ICP-MS line scans of Bi diffusion in basalt (at 1300 °C for 1hr). Open squares are Bi diffusion into air (out top of capsule), black diamonds are Bi diffusion into Pt wall. Dominant diffusion processes is into air.

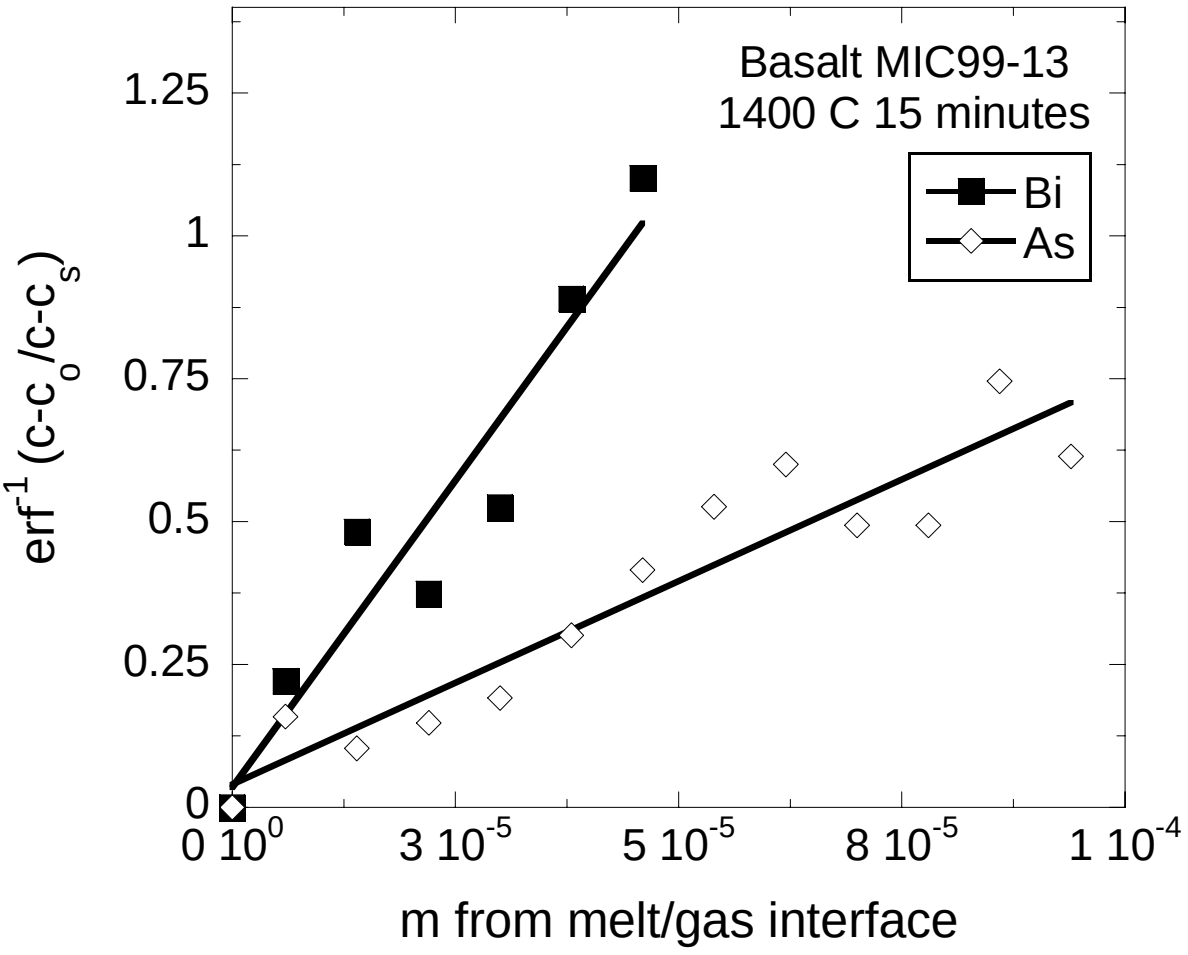

Figure 3.5. Inverse error function of ($c-c_o/c-c_s$) versus distance for Bi and As from which Log*D* is extracted.

profiles (As, Cd, Re, Au, Tl, Pb, Bi). Log*D* varies as a function of temperature and melt composition.

Results show Au and Tl (elements bracketing the location of Hg in the periodic table) are the most volatile in dacite and rhyolite where $\mathrm{Log}D^{\mathrm{Dac}}_{\mathrm{Au}} = -10.7 \pm 0.1$ m^2/s, $\mathrm{Log}D^{\mathrm{Rhy}}_{\mathrm{Au}} = -10.9 \pm 0.1$ m^2/s, $\mathrm{Log}D^{\mathrm{Dac}}_{\mathrm{Tl}} = -10.9 \pm 0.1$ m^2/s and $\mathrm{Log}D^{\mathrm{Rhy}}_{\mathrm{Tl}} = -11.2 \pm 0.3$ m^2/s. The *D* for Au could not be measured in basalt since it volatilized away even in 5 minute experiments, but Tl was similar to dacite and rhyolite, with $\mathrm{Log}D^{\mathrm{Bas}}_{\mathrm{Tl}} = -10.8 \pm 0.2$ m^2/s. In all three starting compositions, elements followed the same decreasing order of volatility: Au, Tl, As , Re, Cd, Pb, Bi (Fig. 3.6).

Diffusivities in rhyolite were slower than diffusivities in dacite, as would be expected in a higher polymerized melt, however, differences between basalt and dacite or basalt and rhyolite were not as pronounced. I was better able to consistently constrain diffusion coefficients in dacite and rhyolite and therefore measure more element diffusivities than in basalt. Diffusivities in dacite spanned two orders of magnitude, whereas diffusivities in rhyolite and basalt spanned 3 orders of magnitude.

A typical Arrhenius plot of diffusion coefficients versus inverse absolute temperature from which activation energies (E_a) and frequency factors (D_o) were extracted is plotted in Figure 3.7 (all element Arrhenius plots are in Appendix I). Activation energies are a representation of the general ease at which an element may move through a melt structure at any given temperature, and a higher E_a (steeper slope) indicates a greater dependence on temperature. This is evident in Cd diffusion in basalt yielding $E_a{}^{\mathrm{Bas}}_{\mathrm{Cd}} = 253.2 \pm 62$ kJ/mol, and $E_a{}^{\mathrm{Dac}}_{\mathrm{Cd}} = 101.0 \pm 18.9$ kJ/mol and $E_a{}^{\mathrm{Rhy}}_{\mathrm{Cd}} =$

54.4 kJ/mol in dacite and rhyolite respectively. Essentially Cd has a lesser dependence on temperature in rhyolite as opposed to basalt melt.

3.5.3. Effects of Ligands

Experimental runs with and without Cl or S are summarized in Table 3.4. For direct comparison, these experiments were run at the same time (e.g. all three (doped basalt, doped basalt + Cl, doped basalt + S) at 1400 °C 15 minutes). Results show Cl and S both increased metal liberation (including Cu, Mo, Sn and Sb) but S had more of an impact on all metals. Figure 3.8 shows the effect of Cl and S on Re and Sb mobility. Cd and As exhibited similar diffusion profiles as Re, and all other metals (Cu, Mo, Sn, Pb, Bi) had the same flat, incrementally decreasing profile as Sb. No comparison could be made for Au and Tl which volatilized away during all comparison experiments.

Diffusion profiles developed in two Cl-bearing basalt experiments, however no S diffusion profiles developed. Figure 3.9 shows an inverse error function plot from which D_{Cl} was extracted in basalt yielding $\text{Log}D_{Cl} = -8.66 \pm 0.1$ m^2/s at 1400 °C 15 minutes similar to $\text{Log}D_{Cl} = -8.53 \pm 0.1$ m^2/s at 1360 °C 5 minutes.

3.6. DISCUSSION

Prior to 1960, diffusion coefficients were available for only a few species in silicate minerals, and studies of diffusion in silicate glass melts (similar to this study) were restricted to the alkali and alkali earth metals until the late 1970s (Freer, 1981).

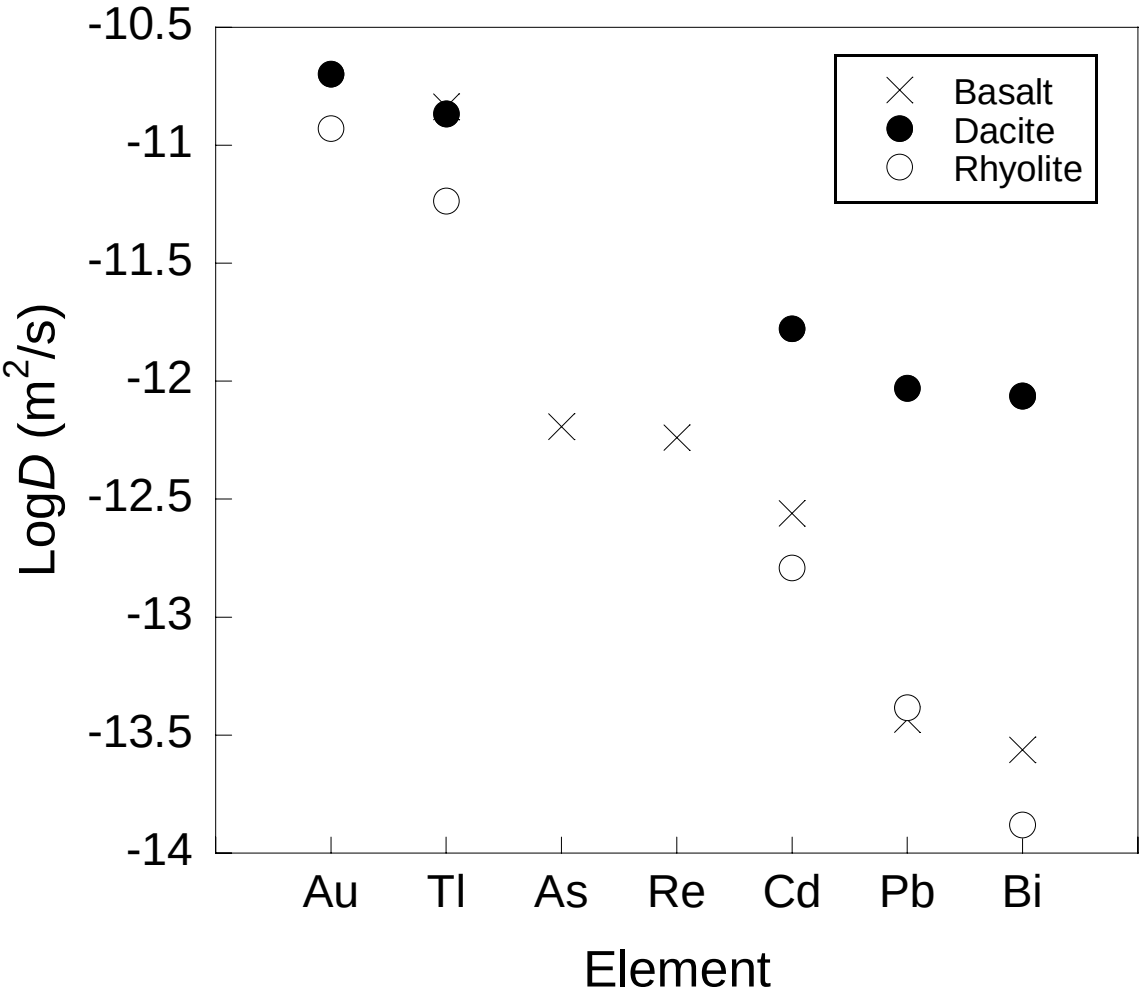

Figure 3.6. Diffusivities of Au, Tl, As, Re, Cd, Pb, Bi (in order of decreasing volatility) in basalt, dacite and rhyolite. Data points are Log*D*s that are either an average of experiments at 1260 °C, or are interpolated based on data points above and below 1260 °C. Log*D*s are not extrapolated outside of experimental results.

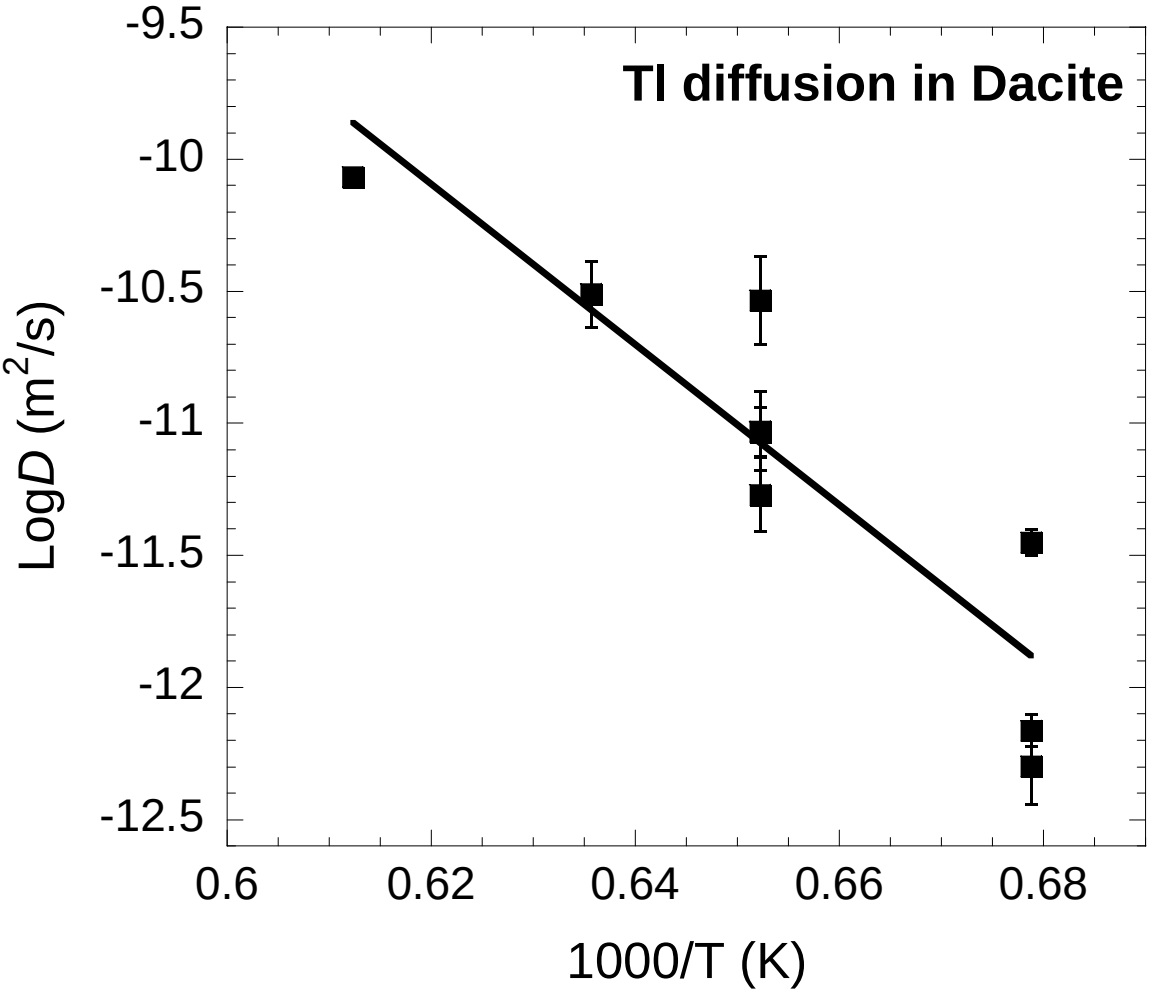

Figure 3.7. Arrhenius plot of Tl in dacite from which activation energies are extracted. Errors on diffusivities are calculated at 1σ.

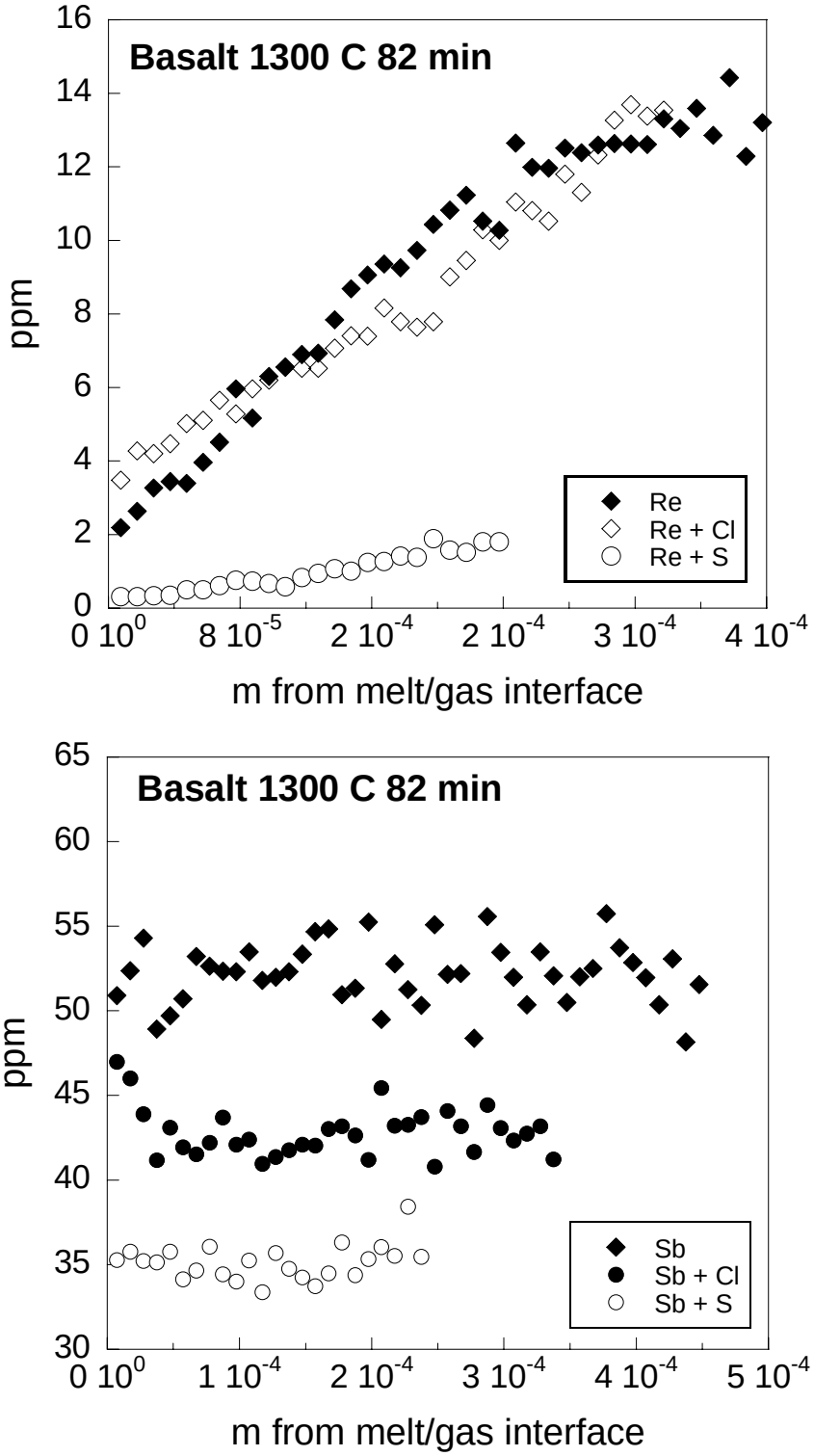

Figure 3.8. Effects of ligands on metal transport. Cd and As exhibited similar diffusion profiles as Re (top) and all other metals (Cu, Mo, Sn, Pb, Bi) had the same flat decreasing profile as Sb (bottom).

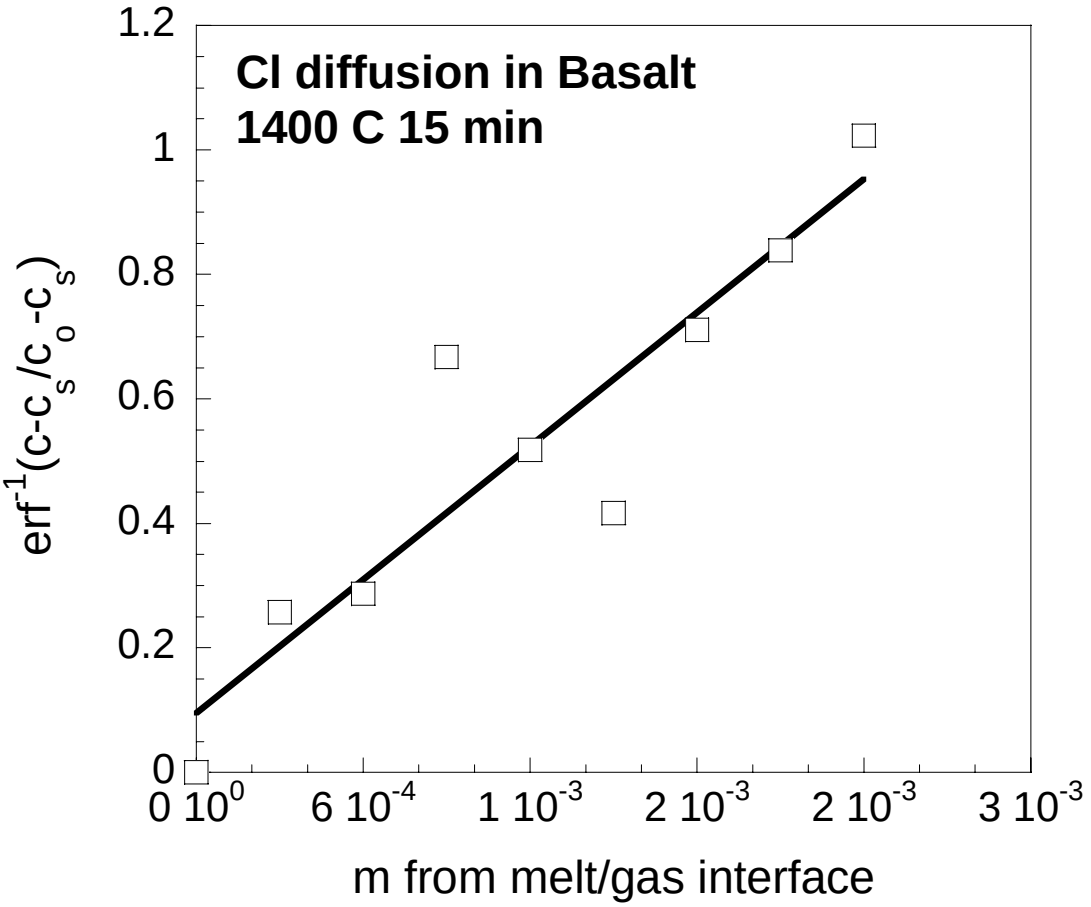

Figure 3.9. Inverse error function plot of Cl diffusion in Basalt at 1400 °C 15 minutes.

Since then, a plethora of studies have been done on diffusion or partition coefficients of the most abundant volatiles in natural and synthetic melts, namely H_2O (e.g. Shaw, 1974; Delaney & Karsten, 1981; Ni et al., 2009), CO_2 (Nowak et al., 2004; Watson et al., 1982), sulfur (Freda, 2005; Simon et al., 2007; Baker & Rutherford, 1996), halogens (Balcone-Boissard et al., 2009; Dingwell & Scarfe, 1985; Aletti et al., 2007, 2009; Webster et al., 1999) and alkali metals (Freda et al., 1998; Bryce et al., 1999; Mungall et al., 1997). Similarly, there is now a large database of diffusion coefficients for metals in synthetic melts in the glass science literature (discussed below).

3.6.1. Diffusion and Melt Structure

Diffusion of a trace metal under a concentration gradient potentially involves interactions amongst many different anionic species in the structural framework of a silicate melt. A silicate melt is an amorphous framework of tetrahedrally-coordinated cations (T) bound by bridging oxygen (BO) and non-bridging oxygen (NBO). Bridging oxygen strongly link or polymerize the tetrahedra, whereas NBO (alkali or metal cations) modify that structure and decrease polymerization (viscosity) of the melt. The ratio of NBO/T represents one way to define polymerization, and represents the electrical charge difference between total negative (O^{2-}) and positive electrical charges of tetrahedrally coordinated cations. Natural magmas exhibit a range of NBO/T from about 0.9 (basalt) to 0.05 (rhyolite) (Mysen et al., 1982) similar to the range of melts investigated in this study. The ease at which a cation migrates through the melt structure is also a result of the melt viscosity, itself related to the melt structure and polymerization (further discussed in 3.6.4). In my experimental design, trace metal cations or ligands that are

part of the melt structure migrate towards the melt/gas interface and are evaporated as oxides at the surface.

3.6.2. Diffusion profiles

Diffusion profiles developed for Cd, As, Re, Au, Tl, Pb and Bi. It is therefore assumed these species were degassed as oxides or complexed with ligands (such as Cl or S) into air. Diffusion profiles rarely or almost never developed for Cu, Mo, Sn and Sb which were also added to the starting materials. These elements remained in the melt at approximately their doped concentrations (except when ligands were added). It could be argued these chalcophile metals simply did not form degassing oxides as they are known to preferentially bind to sulfur. Interestingly, elements for which concentration gradients did not develop, at times exhibited non-uniform, undulating profiles (e.g. Mo in Fig. 3.10) or were essentially flat with too short a diffusion profile to measure meaningfully.

Initially it was assumed that elements not developing compositional profiles (Cu, Mo, Sb, Sn) were simply not being allowed sufficient time to degas. Nonetheless, longer and higher temperature experiments (e.g. rhyolite at 1400 °C for 20 hours) showed identical results in time series plots (e.g. diffusion profiles of Sb at 1400 °C 15 minutes, 4 hours and 20 hours). In other words, Sb = ~50 ppm with a non-uniform undulating profile in all experiments. The addition of ligands (Cl and S) liberated these metals, but still did not show diffusion profiles (Fig. 3.8).

The undulating compositional profiles are metal specific and not due to bubbles quenched in the glass since most other metals were not affected. Tuzzolo & Shelby (1992) discovered crystalline and amorphous colloids of Sb, Bi, and As caused by

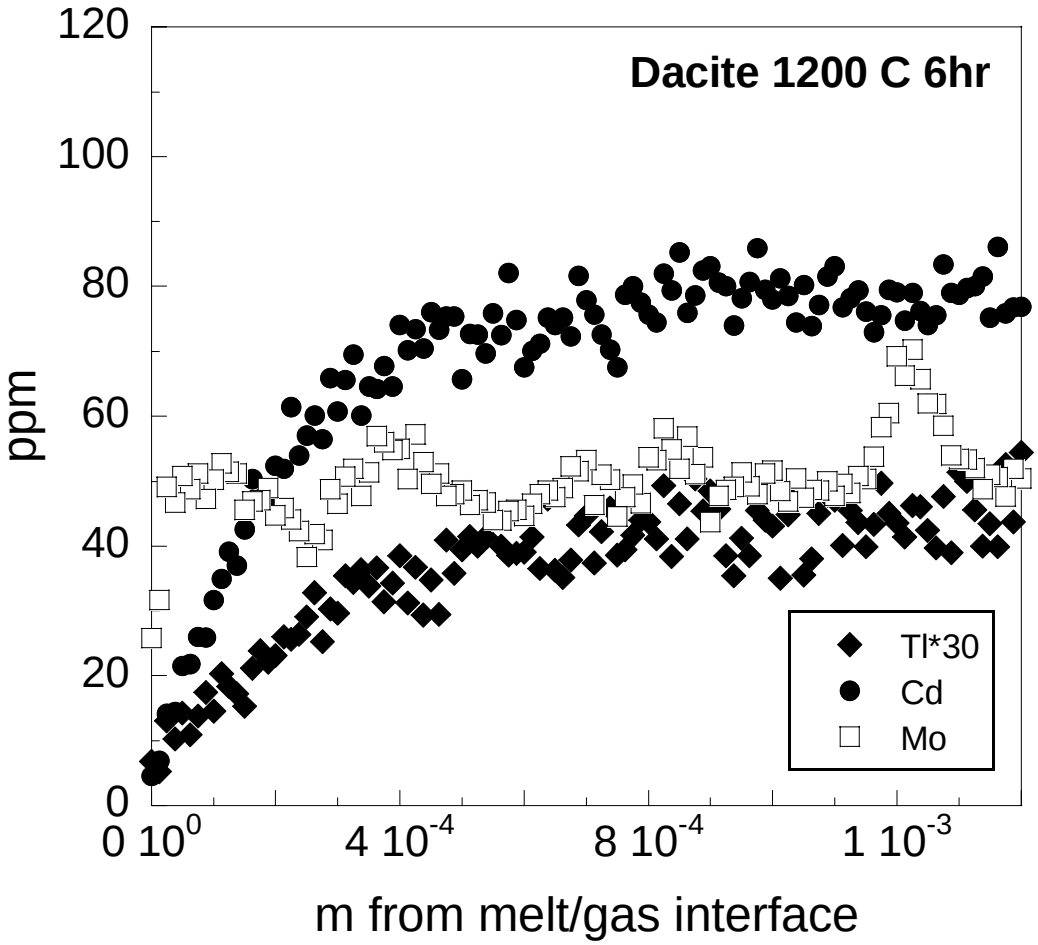

Figure 3.10. Element diffusion profiles from Dacite at 1200 °C, 6hr. Mo exhibits a 'undulating' profile, whereas Tl and Cd show uniform diffusion profiles. Note: Tl concentrations are multiplied by 30 for comparison to other elements.

hydrogen in their study of oxide glasses. This surficial process is thought to be caused by ionic metals diffusing and encountering similar ions to which they nucleate (Shelby, 2005). This nucleation of metal ions may have occurred in my melts, especially if the melt is super saturated with respect to those metals. Another possibility is that clusters or 'nanonuggets' formed in the melt, similar to those in synthetic glasses containing highly siderophile elements (Ertel et al., 2008). It is not known whether these are a quench phenomena or form in the melt at high temperatures due to over-saturation, but this could be an explanation for undulating metal profiles occurring in my experiments when no crystals are present.

3.6.3. Comparison of Diffusion Coefficients

Little to no experimental work has been done on several heavy trace metals in natural systems. Mackenzie and Canil (2008) measured diffusivities of Tl, Pb, Sb, Cd, Te and Re in CMAS (CaO-MgO-Al_2O_3-SiO_2 haplobasalt) and NMAS (Na_2O-MgO-Al_2O_3-SiO_2) compositions but similarly could not measure diffusion coefficients for Cu, Mo or Sn. In general, their diffusivities were one to two orders of magnitude faster than diffusivities measured in this study which would be expected since they used a much lower viscosity, Fe-free, synthetic melt. The only exception is Tl. Tl diffusivities are in close agreement to Mackenzie & Canil (2008) whose $LogD^{CMAS}_{Tl} = -11.0 \pm 0.2$ m^2/s. Mackenzie & Canil (2008) measured essentially identical diffusivities for Tl and Pb ($LogD^{CMAS}_{Pb} = -11.1 \pm 0.2$ m^2/s) whereas diffusivities for Pb in this study are at least two times slower in all three compositions. Mackenzie & Canil (2006) measured Re diffusivities in a natural basalt ($LogD^{Bas}_{Re} = 11.2 \pm 0.2$ m^2/s) which is an order of

magnitude higher than this study ($LogD^{Bas}_{Re} = -12.07 \pm 0.2$ m^2/s). This difference could be due to the smaller Pt capsule used in this study (3 mm O.D.) as opposed to theirs (5 mm O.D.). Basalt creep (up the Pt capsule walls) was sometimes a problem in my experiments, which may have lead to minor convection during the experiment. This could also explain why basalt *D*s are slower than dacite *D*s, even though the opposite would be expected for a less polymerized melt.

3.6.4. Ionic properties and diffusion

Element valences in melts from this study were not measured by voltametric or other means. Therefore, I have assumed the elements are in their most common lowest valence state in oxidizing conditions, and are liberated from the melt as oxides, or complexed with Cl or S. The idea that diffusivities may be predicted based on ionic radii or ionic charge has been explored by many workers (e.g. Hofmann & Brown, 1976; Hofmann, 1980; Jambon et al., 1982 etc.). It is intuitive to think of diffusion being more inhibited by a large, lower charged species such as Tl^{1+} attempting to migrate through the melt structure as opposed to a small, highly charged one such as Re^{6+}. As per numerous investigative studies into this topic, and findings from this study, it is inherently more complex than this.

In general, there are a few simple correlations between ionic radius, ionic charge and diffusion, but no purely quantitative theory is possible (Chakraborty, 1995; Hofmann, 1980). According to Hofmann (1980) (1) diffusivity decreases with increasing radius (2) diffusivity decreases with increasing ionic charge, which is responsible for the failure of Stokes-Einstein's theory. For example, diffusion coefficients for V^{5+} are two times

smaller than diffusion coefficients for Na^+ at 1300 °C even though V has the higher charge and smaller ionic radius. This is explained by the increase in binding forces associated with higher charged ions.

Further to generalizations put forth by Hofmann (1980), Henderson (1985) concluded (1) univalent ion diffusivities (e.g. Tl^+, Na^+) linearly decrease with increasing ionic radius, therefore it should be possible to predict diffusivities of such ions (2) ionic radius has little to no effect on divalent and trivalent ions (3) diffusivities decrease with increasing ionic charge for ions with same or similar ionic radii. In general, attempts to correlate diffusion and ionic parameters in this study proved futile. Tl was the only element that followed a relationship with charge and radius as it was one of the fastest diffusing species and has the largest ionic radii and lowest charge.

3.6.5. Comparison to Glass Science Literature

The glass science literature focuses on diffusion of volatile heavy metals in simple systems (borosilicate melts, alkali and soda-lime silicate melts) over a range of temperatures (600 – 1500 °C) for industrial purposes. According to Claussen & Russel (1997) a direct correlation of diffusion coefficients (D) or activation energies (E_a) with atomic radius, electronegativity or field strength is not possible. In general, diffusion coefficients measured in this study are two to three orders of magnitude slower than diffusivities from the glass science literature in borosilicate or alkali melts (when compared at 1260 °C) (Fig. 3.11). This would be expected since diffusivities are expected to decrease with increasing alkali content and melt polymerization. In the same way, diffusivities measured by von der Gonna & Russel (2000) in a Na_2O-$2SiO_2$

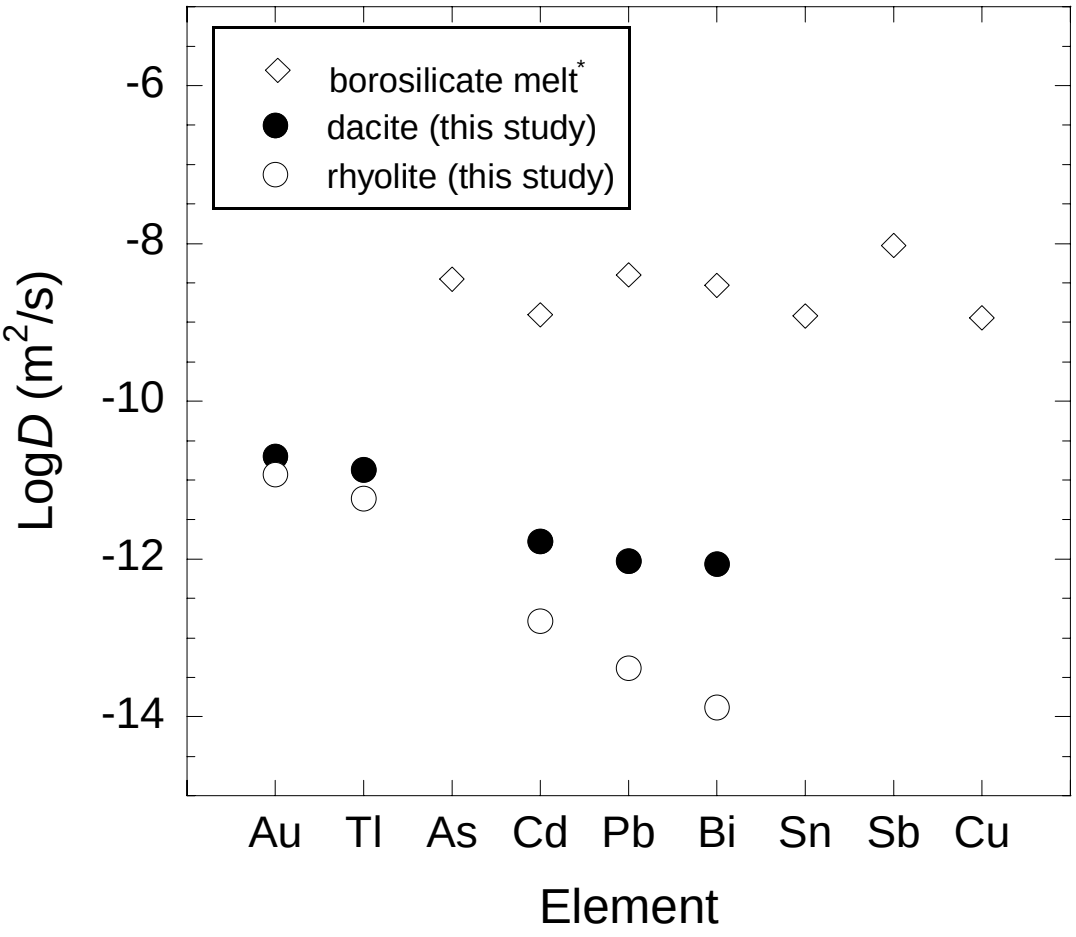

Figure 3.11. Comparison of diffusion coefficients at 1260 °C from this study (circles) to a borosilicate melt (open diamonds) from *Claussen & Russel (1997).

composition are two orders of magnitude slower than diffusivities measured by Claussen & Russel (1997) in a simple borosilicate glass melt.

3.6.6. Effects of Ligands

Ligands such as Cl and S act as transport agents in liberating metals from magma to the vapour phase. Currently, the quantitative effect of Cl and S on the diffusivities of metals (including the ones in this study) are not known, however, Mackenzie & Canil (2006) found evidence to suggest Re complexes with Cl to be liberated from melt as a chloride species. Similarly, all metals in this study had a higher affinity for the vapour phase when Cl and especially when S were added to the melt (Fig. 3.12).

The addition of ligands liberated metals such as Cu, Mo, Sn and Sb that were generally immobile in prior experiments (without ligands). Results confirm chalcophile (e.g. Cd, Pb, As, Bi, Cu, Sn, Sb) and siderophile elements (e.g. Re, Mo) preferentially partition into sulphide phases (Jugo et al., 2005). No direct experimental comparisons could be found in literature to validate or discredit measured Cl diffusivities in basalt at 0.1 MPa. Aletti et al. (2006) measured Cl diffusion at 1250 °C 0.5 GPa in an anhydrous basalt $\text{Log}D_{\text{Cl}} = -10.72$ m^2/s, which is 2 orders of magnitude slower than this study, which is likely due to pressure differences.

3.6.7. Emanation Coefficients

Emanation coefficients (ε_x) are a simple relative measurement of element volatility

$$\varepsilon_x = (C_i - C_f)/C_i$$

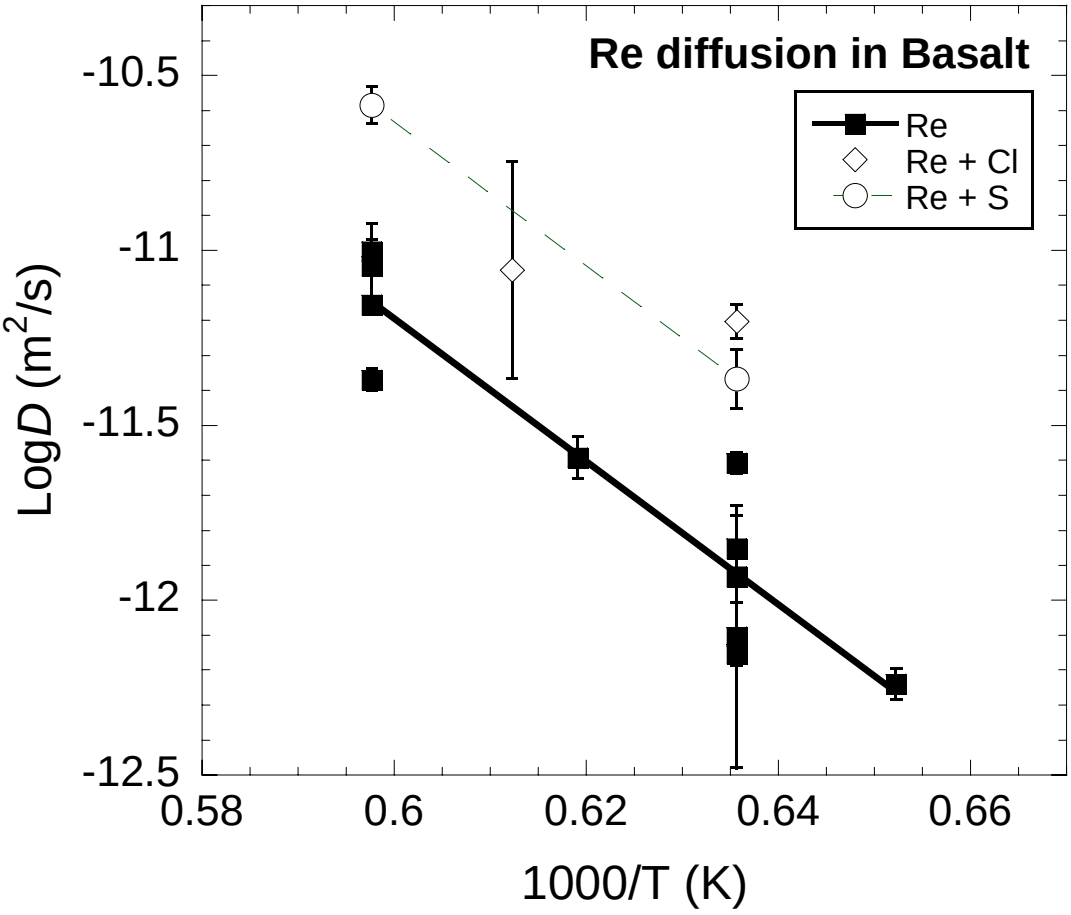

Figure 3.12. Arrhenius plot of Re diffusion with added Cl and S. Error are calculated at 1σ.

where C_i is the initial concentration of metal *x* in the magma before eruption, and C_f is the final concentration of metal *x* after eruption (Lambert et al., 1985). Emanation coefficients range from 0 (completely non-volatile) to 1 (completely volatilized from erupting magma) to compare volatilities of elements. Rubin (1997) compiled volcanic gas data and estimated metal emanation coefficients for eruptions. In general, the proposed trend is such that most volatile elements (B, Bi, Se) have $\varepsilon_x \approx 0.3 – 0.35$, and least volatile elements such as Mg ε_x = 3.9E-07. It is interesting to point out that Hg, which is accepted as one of the most volatile elements with the lowest boiling point at STP (357 °C) has, according to Rubin (1997), a lower emanation coefficient (Hg ε_x = 0.079) than Cd, Re, Se, Bi and B. Gold (Au) sits directly below Hg (Au ε_x = 0.019) and Tl (Tl ε_x = 0.0022) falls below Pb (Pb ε_x = 0.015).

Figure 3.13 is a plot of predicted emanation coefficients from Rubin (1997) and measured diffusivities in basalt at 1260 °C from this study for volatility comparison. My estimated element volatilities differ from Rubin (1997) by having Au and Tl above Pb, Bi, Cd and Re.

Gauthier & Le Cloarec (1998) proposed new emanation coefficients for Tl and other volatile metals from a five year study of Mt. Etna covering multiple stages of varying volcanic activity. They concluded Tl is one of the most volatile metals known with an emanation coefficient higher than 20% when referenced to Pb, following Pennisi et al. (1988). They also noted Tl was approximately 2 – 3 times more volatile than Pb, Bi, Re, As and Cd in basalt which is in agreement with my experimental results. Recently, Baker et al. (2009) compiled Tl emissions (particulate and condensate) from over 32 volcanic gas data sets and similarly concluded that Tl is significantly more

volatile than Pb in the production of volcanic gases. Likewise, Hinkley et al. (1994) confirms Tl and Cd are especially more abundant than other metals in volcanic plumes from Kilauea. The exceptional high volatility of Tl is due to its monovalent, highly incompatible nature which allows it to complex as a sulphide, chloride, oxide or hydroxide species (Churakov, 2000; Baker et al., 2009).

My experiments were conducted in a simplified system, at atmospheric pressures, constant temperatures and with limited investigation into effects of ligands (Cl, S). In nature, magma chambers are in constant motion, either expanding with ascent, convecting, or erupting. Any, or all of these variable could be the reason for differences between my experimental volatility estimates and those measured in nature. Volatile metals are not simply degassed into air, they are partitioned into hydrous fluids containing a complex composition of varying volatiles at different oxygen fugacities which are essentially impossible to replicate in lab. It is possible these variables affect metal diffusion more than we currently understand, however, my measurements are a first order approximation and are in agreement with other studies from nature which suggest Tl is orders of magnitude more volatile than Pb.

3.7. APPLICATION

Volcanic eruptions embody the most efficient mass transfer of volatile species from the mantle to the exosphere (Balcone-Boissard et al., 2009). The primary application of this work, however, is magmatic degassing in volcanic systems. A better understanding of metal fractionation (or mobility) that leads to certain metal ratios in

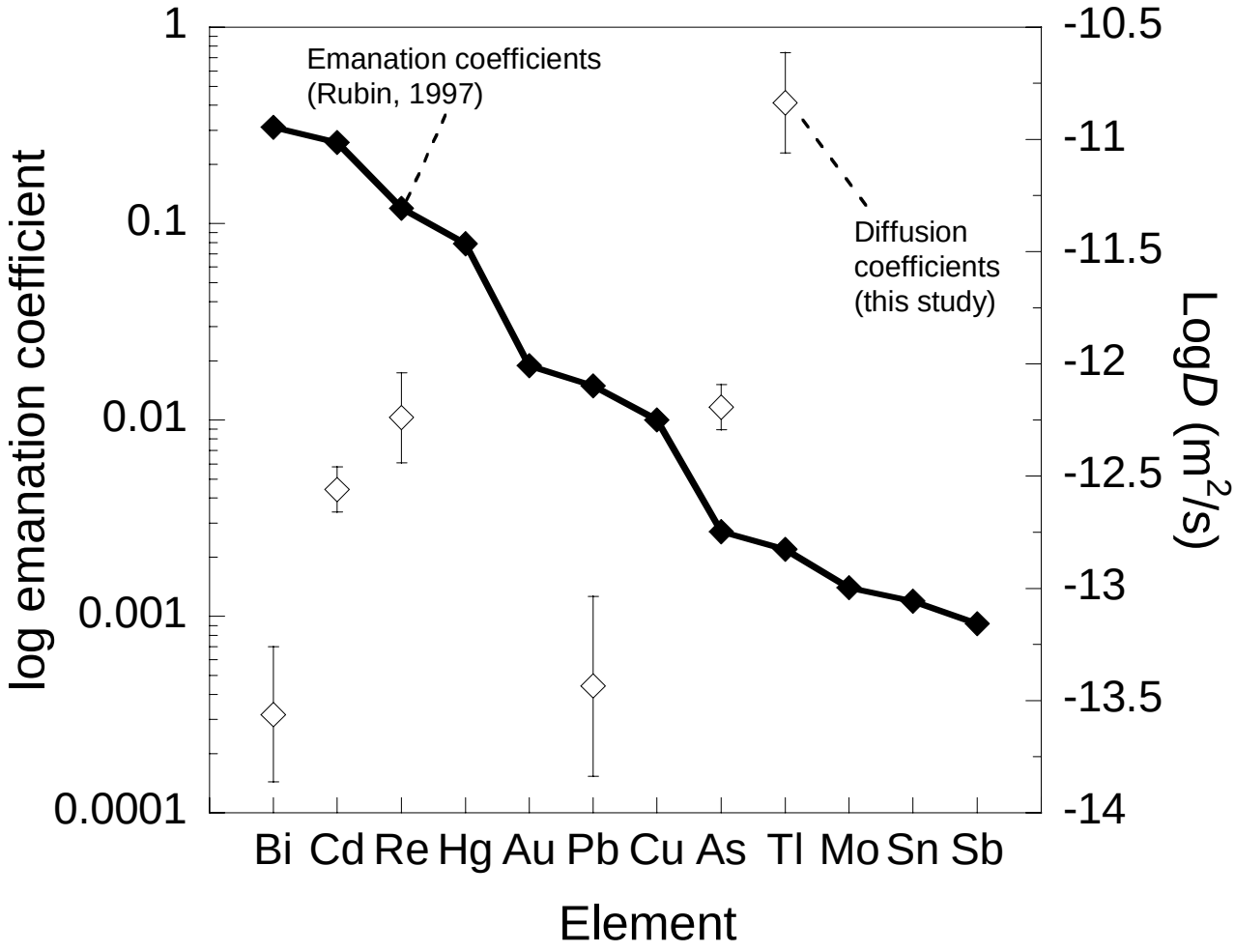

Figure 3.13. Log emanation coefficients (from Rubin, 1997) and basalt Log*D* (this study). Tl is the most volatile in this study, but plots below Pb in Rubin (1997).

volcanic plumes that can be measured at the surface may be useful in eruption prediction.

Numerous studies have confirmed changes in metal fluxes from volcanoes can correspond to changes in the level of eruptive activity (Allard et al., 2000; Perez et al., 1997; Aletti et al., 2007, 2009 etc.). It is widely accepted that relatively rare metals in the crust are in such high abundances in volcanic gas that they commonly have the status of minor or major elements, and typically equal or exceed major rock forming alkali metals (Hinkley et al., 1994, 1999).

Volatile metals degas as a function of (1) the solubility of gas in the magma (2) the nucleation and formation of bubbles, and (3) the efficiency at which gas partitions from melt to bubble (Gardner et al., 1999). Bubble growth in magmas has long held the interest of petrologists. Verrhoogen (1951) first suggested the importance of bubble growth, vesiculation, and coalescence in explosive volcanic eruptions. Sparks (1978) was one of the first papers to incorporate diffusion data into the stationary bubble model of Epstein & Plesset (1950). Bubble growth in magmas is a promising application for data pertaining specifically to diffusion of dissolved volatiles (Watson, 1994).

3.7.1. Bubble Growth Model

Using Smith (1955) simple 1D spherical bubble growth model (similar to Mackenzie & Canil, 2008) I attempt to model metal fractionation as a function of bubble growth rate, partition coefficients and diffusivities of Tl and Pb measured in this study:

$$Cb(r) = \frac{1}{2k} Co\left\{1 + erf\left(\sqrt{\frac{(R/D)r}{2}}\right) + (2k-1)e^{-kq(R/D)r}\, erfc\left(\frac{(2k-1)\sqrt{(R/D)r}}{2}\right)\right\} \quad (3.4)$$

where *Cb* is the concentration of the bubble at some radius (*r*). *Co* is the initial concentration in the melt, *R* is the growth rate, *D* is the diffusion rate, *k* is the partition coefficient and *q* is equal to 1 - *k*. The only available partition coefficients for Tl and Pb are $k_{Tl} = 4.5 \pm 1.4$ and $k_{Pb} = 2.4 \pm 1.8$ (Mackenzie & Canil, in press.). With estimated diffusion and partition coefficients in place, I varied bubble growth rate (*R*) as a function of bubble radius to observe Tl and Pb partitioning into a growing bubble (Fig. 3.14).

Model results indicate that Tl becomes significantly more enriched than Pb as a bubble in magma grows and ascends. Growth rate (*R*) influences the time when Tl/Pb ratios increase. A fast growth rate (10^{-4} cm/s) will become enriched in Tl faster, whereas the opposite is true for a slower growth rate. Given sufficient time, however, all bubbles pass a critical threshold where Tl exponentially becomes enriched relative to Pb. Diffusion coefficients play a critical role in a volatile species diffusing to a growing bubble, and partition coefficients dictate the rate at which this enrichment occurs. Subsequently, Tl is predicted to be more enriched in volcanic plumes as opposed to Pb when measured at the surface.

Gauthier & Le Cloarec (1998) observed up to three orders of magnitude enrichment of Tl at Mt. Etna effusive vents relative to summit crater lava flow eruptions. The latter are typically degassed lavas (assuming degassing takes place under the crater before eruptions). In this way, Tl enrichment in volcanic plumes may indicate fresh undegassed magma has entered the system.

Elements with high volatility are likely to be the best candidate for indicating when fresh undegassed magma has entered a volcanic system. Perez et al. (1997) observed an increase in Hg/S molar ratios in the months prior to a Strombolian eruption

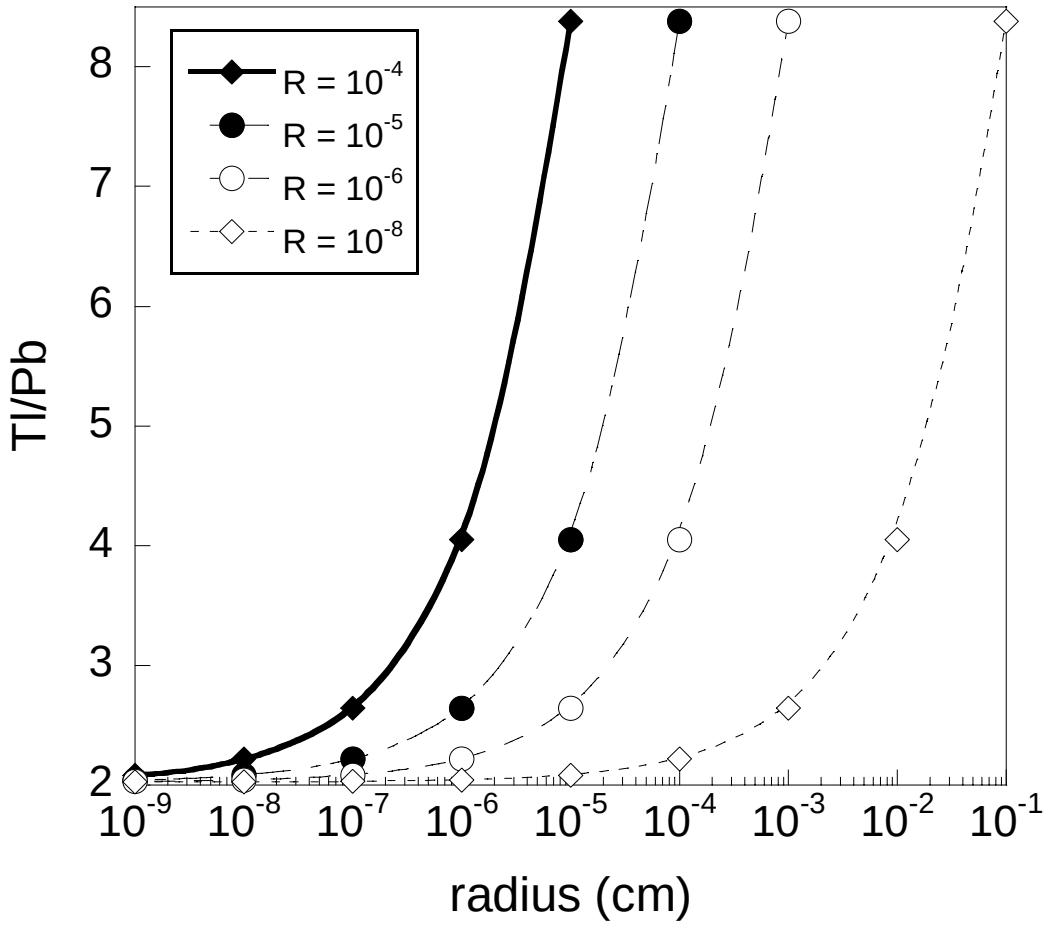

Figure 3.14. Plot of log Tl/Pb concentration as a function of bubble growth rate (*R* in cm/s) using diffusion coefficients (*D*) from this study and partition coefficients (*k*) from Mackenzie & Canil (in press).

at Tavurvur volcano, Papua New Guinea and a fall in As/S ratios were coincided with the frequency and style of eruption at Mt. Erebus (Wardell et al., 2008). Also, empirical observations of an increase in Cd/Re and Cd/Sb ratios directly before an eruption have been observed (Crowe et al., 1987) and can be explained as a result of varying diffusivity (Mackenzie & Canil, 2008).

The bubble growth model employed here simplifies the process of element fractionation into a bubble ascending in a magma chamber. Variables such as surface tension, changes in pressure, magma mixing/convection, bubble coalescence or interaction with the 'froth layer' (build up of gas bubbles) at the top of a magma chamber are not considered here, but have been attempted by other workers. Proussevitch et al. (1993) modeled inter-bubble coalescence and diffusion of species through the 'froth' layer. They observed a number of factors including various bubble sizes, film thickness, temperature, external pressure, and gas solubility in the melt modulate these processes, most of which are outside the scope of this thesis.

Volcanic gas data reflects the chemical composition of the magma from which it is liberated (Hinkley, 1994). There are major variations in magma composition between volcanoes, which will ultimately lead to variations in volatile abundances. These variations may be a direct result of tectonic setting. For example, Mt. Etna is known as a high S volcano whereas Mt. Erebus, an intraplate volcano, has a unique elemental gold signature (Hinkley et al., 1999). Kilauea has hot spot characteristics of high F and heavy metals such as Ir, since it taps deep, undepleted mantle (Olmez et al., 1986). Perhaps different volcanoes will have different metal ratios or metal/halogen ratios to indicate pending activity. This then requires volcano specific research, experiments and

monitoring. Similarly, depending on time of sampling, the magma chamber may have exhausted its most volatile elements, therefore a suite of metals may useful to identify what stage of degassing a magma chamber is currently at.

If certain element ratios are to be utilized for predicting volcanic eruptions, real time gas data must systematically capture such enrichments directly before volcanic activity at a statistically meaningful number of volcanoes. Real-time gas data for pre-, syn- and post eruption metal emissions is sparse, and while lab investigations are imperative to measure element volatility, ultimately, to apply this data to nature and propose a convincing argument in forecasting eruptions, one requires real-time gas data from nature to support such claims. Ideally, we will be able to correctly identify specific metal ratios that can be applied to volcanoes around the world. This requires continued experimental studies, and ongoing collection of volcanic gas data.

3.7.2. Volcanogenic fluxes and metal proxies

Even with renewed interest in heavy metal transport due to environmental impacts, there is still a large gap in our knowledge and understanding of how heavy metals behave in igneous systems in their volatile form during volcanic degassing. Significant uncertainties arise in global volcanogenic fluxes given that real-time metal measurements are costly and dangerous (especially at explosive volcanoes) and trace metal fluxes are typically estimated based on normalizing with reference to SO_2. Calculation problems lie in what percentage of Tl, Pb or Hg, for example, is present in the gaseous or particulate form.

This study addresses the mobility of heavy metals diffusing towards the melt/gas interface at high temperatures. Volcanic gas measurements, however, are made at atmospheric pressures and temperatures, sometimes tens of meters from which the element was initially liberated from the magma. Most gaseous metals en route to the surface are likely scavenged onto particles (dust, ash) as they cool or as they are transported in plumes (Hinkley et al., 1991, 1999). Gauthier & Le Cloarec (1998) observed nearly all of Tl and Pb is complexed to S-rich particles, however, the initial gaseous ratio of Tl/Pb persisted and subsequently was still measured in their study.

This work may help better constrain the behavior/mobility of toxic metals which are difficult to constrain in nature such as Hg using Au or Tl as a proxy. Au and Tl were considerably the most volatile heavy metals measured in this study and bracket Hg on the periodic table. Au and Tl are roughly in the same abundances as Hg when measured in volcanic plumes (0.1 - 30 ppb (Gemmell, 1987; Yudovskaya et al., 2008; Hedenquist et al., 1994) the large range is due to volcano to volcano element emission variations and measuring techniques). Churakov et al. (2000) modeled metal transport and similarly suggested the positioning of Au and Ag on the periodic table may indicate they have similar properties to Cd and Hg. I suggest Au and Tl are the best known proxy for Hg degassing from a magma.

3.8. SUMMARY

I have investigated the volatile behavior of Au, Tl, Pb, Cd, Re, As, Cu, Mo, Sn, Sb and Bi in natural basalt, dacite and synthetic rhyolite at 0.1 MPa. Diffusion profiles

did not develop for Cu, Mo, Sn or Sb, however, diffusion coefficients were measured for Au, Tl, As, Re, Cd, Pb, Bi and Cl. Affects of ligands Cl and S were investigated and shown to significantly increase the rate at which all metals are liberated from the melt. Diffusivities were shown to be temperature and melt composition dependent and follow the Arrhenius equation from which activation energies (E_a) and frequency factors (D_o) were extracted.

Experimental results confirm diffusivities between metals can span three orders of magnitude, and a simple bubble growth model shows a first approximation of such fractionation processes occurring at depths for Tl and Pb. In this way, metal enrichment measured at the surface may be explained by diffusion and partition coefficients in ascending bubbles. My experiments show Tl and Au are the most volatile metals, and as such, will likely be enriched in volcanic plumes (relative to less volatile metals such as Pb) if an injection of fresh magma to the magma chamber is degassing. Tl and Au may be likely candidates to use as a proxy for Hg in volcanic flux estimates due to their position beside Hg on the period table and similar high affinity for the vapour phase. I propose Tl/Pb ratios in volcanic plumes (in conjunction to other metal ratios such as Cd/Re or Hg/S) have potential to indicate impending volcanic activity.

Table 3.1. Major element chemical compositions of starting materials

	Basalt doped	Dacite doped	Rhyolite doped
Oxide	wt%	wt%	wt%
Na_2O	1.8	4.5 (0.2)	2.9 (0.5)
MgO	7.6	1.3	
Al_2O_3	13.5	15.2 (0.2)	10.8 (1.8)
SiO_2	49.0 (0.3)	67.7 (0.4)	79.9 (3.1)
K_2O	0.1	2.6	5.4 (0.5)
CaO	12.2	3.1	1.0 (0.3)
TiO_2	1.3	0.5	
MnO	0.2	0.1	
Fe_2O_3	13.6 (0.2)	3.3 (0.2)	
Total	99.4 (0.5)	98.1 (0.5)	100 (0.4)

Values are 15 measurements on randomly selected glass chips.
1σ standard deviations are ≤ 0.1 unless otherwise stated in brackets.

Table 3.2. Trace element concentrations of heavy metal doped natural and synthetic starting materials (LA-ICP-MS analysis).

Element	Basalt doped (ppm)	Dacite doped (ppm)	Rhyolite doped (ppm)
Cu	93.6 (112.5)	67.1 (50.0)	119.2 (65.5)
As	38.6 (6.2)	68.9 (9.1)	27.4 (10.6)
Mo	24.6 (1.6)	60.0 (9.4)	17.8 (11.3)
Cd	34.7 (23.6)	85.0 (7.1)	80.6 (59.3)
Sn	14.9 (6.1)	12.5 (11.3)	81.6 (32.1)
Sb	46.0 (22.8)	9.7 (12.6)	67.5 (32.0)
Yb	2.6 (0.2)	1.4 (0.2)	0.7 (0.4)
Re	6.7 (1.9)	29.4 (26.1)	6.7 (4.2)
Au	21.0 (6.7)	28.7 (15.9)	16.2 (5.4)
Tl	0.5 (0.2)	1.2 (0.3)	0.4 (0.7)
Pb	18.0 (4.8)	28.0 (5.3)	79.5 (39.2)
Bi	28.1 (6.8)	15.6 (12.6)	80.5 (29.2)

Values are 5 measurements on randomly selected glass chips.
1σ standard deviations are in brackets.

Table 3.3. Calculated Log*D*s at 1260 °C, activation energies (E_a) and frequency factors (D_o) of elements in this study.

Element	Basalt Log*D* (m^2/s)	Error	*Ea* (kJ/mol)	Error	log*Do* (m^2/s)	Error
Tl	-10.8	0.2				
As	-12.2	0.1	154.9	5.8	0.1	0.4
Re	-12.2	0.2	170.1	22.2	1.1	1.7
Cd	-12.6	0.1	253.4	61.6	7.1	4.6
Pb	-13.4	0.4				
Bi	-13.6	0.3				
	Dacite Log*D* (m^2/s)	Error	*Ea* (kJ/mol)	Error	log*Do* (m^2/s)	Error
Au	-10.7	0.1	150.3	12.6	1.2	1.0
Tl	-10.9	0.1	251.9	55.3	8.7	4.4
Cd	-11.8	0.1	101.0	18.9	-3.9	1.5
Pb	-12.0	0.2	106.5	25.7	-7.6	2.0
Bi	-12.1	0.1				
	Rhyolite Log*D* (m^2/s)	Error	*Ea* (kJ/mol)	Error	log*Do* (m^2/s)	Error
Au	-10.9	0.1	202.5	54.2	5.0	4.2
Tl	-11.2	0.3	175.9	30.1	3.2	2.3
Cd	-12.8	0.1	58.3	12.6	-8.2	0.9
Pb	-13.4	0.1	139.4	9.3	-2.5	0.7
Bi	-13.9	0.6	218.5	71.3	3.2	5.3

Values of Log*D* are experimental data points at 1260 °C or were interpolated based on data above and below 1260 °C. Log*D*s were not extrapolated outside of experimental run temperatures. Errors are calculated at 1σ.

Table 3.4. Summary of experimental run conditions. *D* is calculated from slope of erf^{-1} versus distance (Fig. 3.4).

Basalt (MIC99-13)

Element	T (°C)	T (K)	1000/K	duration (hr)	*D* (m^2/s)	Error	log*D* (m^2/s)	Error
As	1260	1533.15	0.65	1.5	5.41E-13	5.40E-14	-12.3	0.1
As	1300	1573.15	0.64	2	1.34E-12	1.55E-13	-11.9	0.1
As	1300	1573.15	0.64	4	1.27E-12	1.83E-13	-11.9	0.1
As	1300	1573.15	0.64	5 min	2.24E-12	8.11E-13	-11.7	0.2
As	1300	1573.15	0.64	1.36	4.02E-12	3.77E-13	-11.4	0.1
As	1400	1673.15	0.60	0.25	6.69E-12	9.85E-13	-11.2	0.1
As	1400	1673.15	0.60	0.25	6.02E-12	7.66E-13	-11.2	0.1
As	1400	1673.15	0.60	0.25	1.52E-11	2.20E-12	-10.8	0.1
As	1400	1673.15	0.60	0.5	7.59E-12	1.95E-12	-11.1	0.1
As + Cl	1300	1573.15	0.64	1.36	2.18E-12	5.14E-13	-11.7	0.1
As + Cl	1400	1673.15	0.60	0.25	1.80E-11	2.07E-12	-10.7	0.1
As + S	1300	1573.15	0.64	1.36	3.88E-12	1.03E-12	-11.4	0.1
As + S	1400	1673.15	0.60	0.25	9.88E-12	1.27E-12	-11.0	0.1
Cd	1260	1533.15	0.65	1.5	2.76E-13	5.91E-14	-12.6	0.1
Cd	1300	1573.15	0.64	6	2.35E-13	7.04E-14	-12.6	0.1
Cd	1300	1573.15	0.64	5 min	8.14E-13	3.94E-13	-12.1	0.2
Cd	1342	1615.15	0.62	1	5.12E-13	1.27E-13	-12.3	0.1
Cd	1400	1673.15	0.60	0.25	5.47E-12	9.36E-13	-11.3	0.1
Cd	1400	1673.15	0.60	0.25	1.06E-11	1.27E-12	-11.0	0.1
Cd	1400	1673.15	0.60	0.5	2.36E-11	1.45E-11	-10.6	0.3
Cd	1430	1703.15	0.59	0.25	9.92E-12	2.95E-12	-11.0	0.1
Cd + Cl	1400	1673.15	0.60	0.25	4.93E-11	6.14E-12	-10.3	0.1
Cd + Cl	1400	1673.15	0.60	0.25	9.88E-12	2.17E-12	-11.0	0.1
Cd + S	1400	1673.15	0.60	0.25	6.53E-12	1.92E-12	-11.2	0.1
Re	1260	1533.15	0.65	1.5	5.76E-13	5.85E-14	-12.2	0.1
Re	1300	1573.15	0.64	1.5	1.41E-12	3.03E-13	-11.9	0.1
Re	1300	1573.15	0.64	2	7.04E-13	5.35E-14	-12.2	0.1
Re	1300	1573.15	0.64	4	1.17E-12	2.03E-13	-11.9	0.1
Re	1300	1573.15	0.64	5 min	7.86E-13	6.79E-13	-12.1	0.4
Re	1300	1573.15	0.64	1.36	2.46E-12	1.74E-13	-11.6	0.1
Re	1342	1615.15	0.62	1	2.56E-12	3.56E-13	-11.6	0.1
Re	1400	1673.15	0.60	0.25	9.93E-12	7.57E-13	-11.0	0.1
Re	1400	1673.15	0.60	0.25	6.99E-12	2.43E-13	-11.2	0.0
Re	1400	1673.15	0.60	0.25	4.27E-12	3.10E-13	-11.4	0.1
Re	1400	1673.15	0.60	0.5	9.04E-12	2.50E-12	-11.0	0.1
Re + Cl	1300	1573.15	0.64	1.36	6.27E-12	6.87E-13	-11.2	0.1
Re + Cl	1360	1633.15	0.61	5 min	8.80E-12	6.28E-12	-11.1	0.3
Re + S	1300	1573.15	0.64	1.36	4.29E-12	8.21E-13	-11.4	0.1

Element	T (°C)	T (K)	1000/K	duration (hr)	D (m^2/s)	Error	log$D$ (m^2/s)	Error
Re + S	1400	1673.15	0.60	0.25	2.61E-11	3.27E-12	-10.6	0.1
Tl	1260	1533.15	0.65	1.5	1.46E-11	7.51E-12	-10.8	0.2
Tl	1300	1573.15	0.64	5 min	1.43E-11	7.09E-12	-10.8	0.2
Pb	1260	1533.15	0.65	1.5	3.67E-14	1.10E-14	-13.4	0.1
Pb	1300	1573.15	0.64	5 min	1.87E-12	6.16E-13	-11.7	0.1
Pb	1400	1673.15	0.60	0.25	1.14E-12	3.82E-13	-11.9	0.1
Pb + S	1400	1673.15	0.60	0.25	1.07E-12	1.01E-12	-12.0	0.4
Bi	1260	1533.15	0.65	1.5	2.75E-14	2.06E-14	-13.6	0.3
Bi	1300	1573.15	0.64	5 min	1.86E-12	8.98E-13	-11.7	0.2
Bi	1342	1615.15	0.62	1	2.81E-14	1.24E-14	-13.6	0.2
Bi	1400	1673.15	0.60	0.25	6.03E-13	1.67E-13	-12.2	0.1
Bi + S	1400	1673.15	0.60	0.25	8.25E-13	3.56E-13	-12.1	0.2
Cl	1360	1633.15	0.61	5min	2.94E-09	6.41E-10	-8.5	0.1
Cl	1400	1673.15	0.60	0.25	2.17E-09	7.05E-10	-8.7	0.1

Dacite (Mt. Meager Pumice)

Element	T (°C)	T (K)	1000/K	duration (hr)	D (m^2/s)	Error	log$D$ (m^2/s)	Error
Cd	1200	1473.15	0.68	1	4.97E-13	1.73E-13	-12.3	0.2
Cd	1200	1473.15	0.68	4	1.34E-12	1.44E-13	-11.9	0.1
Cd	1200	1473.15	0.68	10	5.28E-13	6.14E-14	-12.3	0.1
Cd	1260	1533.15	0.65	1	1.59E-12	2.50E-13	-11.8	0.1
Cd	1260	1533.15	0.65	4	2.66E-12	4.53E-13	-11.6	0.1
Cd	1260	1533.15	0.65	4	1.30E-12	2.16E-13	-11.9	0.1
Cd	1260	1533.15	0.65	4	1.43E-12	2.32E-13	-11.8	0.1
Cd	1360	1633.15	0.61	4	5.15E-12	4.40E-13	-11.3	0.1
Cd	1400	1673.15	0.60	0.25	6.39E-12	1.20E-12	-11.2	0.1
Au	1260	1533.15	0.65	0.5	2.17E-11	2.20E-12	-10.7	0.1
Au	1260	1533.15	0.65	1	1.85E-11	8.83E-12	-10.7	0.2
Au	1300	1573.15	0.64	0.25	6.98E-11	7.44E-12	-10.2	0.1
Au	1360	1633.15	0.61	5 min	1.00E-10	2.42E-11	-10.0	0.1
Tl	1200	1473.15	0.68	4	6.88E-13	9.72E-14	-12.2	0.1
Tl	1200	1473.15	0.68	6	3.54E-12	3.95E-13	-11.5	0.1
Tl	1200	1473.15	0.68	10	5.03E-13	1.67E-13	-12.3	0.1
Tl	1260	1533.15	0.65	0.5	2.92E-11	1.12E-11	-10.5	0.2

Element	T (°C)	T (K)	1000/K	duration (hr)	D (m^2/s)	Error	log$D$ (m^2/s)	Error
Tl	1260	1533.15	0.65	4	9.25E-12	1.98E-12	-11.0	0.1
Tl	1260	1533.15	0.65	4	5.37E-12	1.74E-12	-11.3	0.1
Tl	1300	1573.15	0.64	0.25	3.08E-11	8.80E-12	-10.5	0.1
Tl	1360	1633.15	0.61	1	8.56E-11	6.10E-12	-10.1	0.1
Pb	1200	1473.15	0.68	10	5.07E-13	3.96E-14	-12.3	0.0
Pb	1260	1533.15	0.65	4	7.04E-13	8.17E-14	-12.2	0.1
Pb	1260	1533.15	0.65	4	1.38E-12	1.66E-13	-11.9	0.1
Pb	1300	1573.15	0.64	4	1.52E-12	1.98E-13	-11.8	0.1
Pb	1300	1573.15	0.64	6	8.35E-13	8.85E-14	-12.1	0.1
Pb	1300	1573.15	0.64	6	7.99E-13	1.25E-13	-12.1	0.0
Pb	1360	1633.15	0.61	4	4.66E-12	3.50E-13	-11.3	0.1
Bi	1260	1533.15	0.65	4	4.88E-12	2.60E-12	-11.3	0.2
Bi	1260	1533.15	0.65	4	1.54E-13	2.86E-14	-12.8	0.1
Bi	1300	1573.15	0.64	5 min	9.74E-11	9.63E-12	-10.0	0.1

Rhyolite (Ab-Or-Qz)

Element	T (°C)	T (K)	1000/K	duration (hr)	D (m^2/s)	Error	log$D$ (m^2/s)	Error
As	1360	1633.15	0.61	6	2.99E-15	9.36E-16	-14.5	0.1
As	1400	1673.15	0.60	4	1.63E-13	2.91E-14	-12.8	0.1
As	1430	1703.15	0.59	0.25	2.65E-13	5.37E-14	-12.6	0.1
As	1430	1703.15	0.59	3	2.45E-12	1.44E-12	-11.6	0.3
Cd	1200	1473.15	0.68	10	1.06E-13	2.21E-14	-13.0	0.1
Cd	1300	1573.15	0.64	6	1.80E-13	8.60E-14	-12.7	0.2
Cd	1400	1673.15	0.60	0.25	4.97E-13	1.53E-13	-12.3	0.1
Cd	1430	1703.15	0.59	3	3.74E-13	1.13E-13	-12.4	0.1
Au	1260	1533.15	0.65	0.5	1.67E-11	5.00E-12	-10.8	0.1
Au	1260	1533.15	0.65	1	8.34E-12	1.68E-12	-11.1	0.1
Au	1300	1573.15	0.64	5 min	3.29E-11	1.04E-11	-10.5	0.1
Au	1360	1633.15	0.61	5 min	1.11E-10	3.32E-11	-10.0	0.1
Tl	1200	1473.15	0.68	6	2.28E-12	4.66E-13	-11.6	0.1
Tl	1200	1473.15	0.68	10	1.24E-12	3.72E-13	-11.9	0.1
Tl	1260	1533.15	0.65	1	2.49E-12	1.15E-12	-11.6	0.2
Tl	1300	1573.15	0.64	5 min	1.65E-11	5.25E-12	-10.8	0.1
Tl	1360	1633.15	0.61	0.5	2.85E-11	1.05E-11	-10.5	0.2
Tl	1360	1633.15	0.61	4	5.06E-11	1.86E-11	-10.3	0.2

Element	T (°C)	T (K)	1000/K	duration (hr)	D (m^2/s)	Error	log$D$ (m^2/s)	Error
Pb	1260	1533.15	0.65	12	3.37E-14	7.75E-15	-13.5	0.1
Pb	1300	1573.15	0.64	6	8.42E-14	1.52E-14	-13.1	0.1
Pb	1360	1633.15	0.61	6	1.68E-13	3.54E-14	-12.8	0.1
Pb	1400	1673.15	0.60	0.25	3.20E-13	2.76E-13	-12.5	0.4
Pb	1400	1673.15	0.60	4	3.62E-13	5.72E-14	-12.4	0.1
Pb	1430	1703.15	0.59	3	4.06E-13	6.72E-14	-12.4	0.1
Bi	1300	1573.15	0.64	6	2.32E-14	9.00E-15	-13.6	0.2
Bi	1342	1615.15	0.62	1	1.45E-13	9.46E-14	-12.8	0.3
Bi	1400	1673.15	0.60	0.25	4.33E-13	1.79E-13	-12.4	0.2
Bi	1400	1673.15	0.60	4	1.78E-13	1.13E-13	-12.7	0.3

Chapter 4
SUMMARY

The main goal of this thesis was to better constrain the behavior, mobility and speciation of a suite of volatile heavy metals through the analysis of natural volcanic samples and experimental work. Specifically, I investigated how metals behave during diffusion en route to the melt/gas interface as they are liberated from a melt. Natural pumice samples were collected from a dormant volcano (Mt. Meager) for metal analysis, and experiments were conducted in natural and synthetic melts to investigate how these metals were effected by temperature, melt polymerization and the addition of ligands Cl and S.

In my second chapter "The degassing behavior of Hg in subaerially erupted magmas" I found that the most volatile metals such as Hg, As, Cd were in low sporadic concentrations (or were below detection) and did not correlate to any colouration or textural changes found in the pumice bombs. Metals were likely fully degassed during eruption, or were leached/weathered after deposition. Mercury is a unique element, with distinctive physical properties that has major environmental implications. We still lack fundamental knowledge as to its behavior in igneous systems which would greatly benefit from supplemental experimental work (perhaps using its proxy heavy metals Au, Tl as suggested here).

In my third chapter "Experimental investigation of the degassing behavior of Hg via proxy heavy metals in natural and synthetic melts" I measured diffusion profiles and extracted diffusion coefficients for Au, Tl, Re, Cd, Pb and Bi (in decreasing order of volatility) in natural basalt, dacite and synthetic rhyolite. The addition of Cl and S

confirm they complex with all metals and increase their affinity for the vapour phase, especially S. Elements followed an Arrhenius equation from which activation energies and frequency factors were extracted. In all three compositions, Au and Tl were fastest diffusing species and consistently 1 – 3 times more volatile than all the other metals, and 2 – 3 times more volatile than Pb.

I applied the diffusivities of Tl and Pb to a simple 1D bubble growth model (Smith 1955). These elements were chosen due to their orders of magnitude difference in volatility. Model results confirm that Tl becomes more enriched in ascending bubbles relative to Pb during fractionation at a rate controlled by diffusion coefficients, bubble growth rate and partition coefficients. In this way, Tl/Pb ratios measured at the surface are predicted to increase upon an influx of new magma that will degas its most volatile metals first. It is suggested that Tl is one of the most volatile elements (Gauthier & Le Cloarec., 1998) and its enrichment at the surface could indicate impending volcanic activity as fresh magma has entered the system. This suggestion is in good agreement with field observations from Kilauea and Mt. Etna (Hinkley et al., 1999; Baker et al., 2009).

Volcanic eruptions are controlled by volatile exsolution, bubble growth and magmatic ascent/expansion (Villemant, 1999; Shinohara, 2008). Volcanic prediction has made significant advances in recent decades and is the main goal of monitoring/research efforts. Monitoring of trace metals at the surface may provide critical insight into processes occurring at depths in a magma chamber and may ultimately be the key factor in our ability to forecast volcanic eruptions.

FUTURE WORK

While there is a growing number of empirical measurements on metals degassed from volcanic edifices, there is a lag in experimental work on the behavior of most of these elements in geologically relevant systems constrained in the lab.

Melt composition and temperature were shown to have the greatest influence on measured diffusion coefficients. Ligands Cl and S also had a significant impact on the rate at which these metals were liberated from a melt. Further investigations to better constrain these effects would supplement the first order approximations presented here. For example, it would be interesting to see how varying ligand concentration affects diffusion.

Basalt experiments were sometimes subjected to melt creep up the sides of the Pt capsule wall. Basalt diffusion coefficients were still used because they were consistent, however, basalt experiments performed in a wider radius capsule (5 mm or more) might warrant a flatter, more static melt/gas interface that may yield better results.

The effect of oxygen fugacity was not investigated here, however, experiments from Mackenzie & Canil (2006) show it has little to no effect on diffusion of elements. This is not to suggest this avenue should not be explored further. Perhaps in conjunction with experiments at higher pressures. This would yield partition coefficients for which there is also a deficiency of data, and would more closely simulate nature.

A newer model that accounts for surface tension in three-dimensions as well as the incorporation of widely accepted (replicated) diffusion coefficients and partition coefficients that confirm or dispute the findings here would produce more realistic modeling results.

REFERENCES

Aiuppa, A., Federico, C., (2004) Anomalous magmatic degassing prior to the 5th April 2003 paroxysm on Stromboli. Geophysical Research Letters, 31, L14607.

Aiuppa, A., Federico, C., Giudice, G., Gurrieri, S., Paonita, A. Valenza, M. (2004) Plume Chemistry provides insights into mechanisms of sulfur and halogen degassing in basaltic volcanoes. Geophysical Research Letters, 222, 469-83.

Aiuppa, A., Federico, C., Giudice, G., Giuffrida, G., Guida, R., Gurrieri, S., Liuzzo, M., Moretti, R., Papale, P. (2004) The 2007 eruption of Stromboli volcano: Insights from real-time measurement of the volcanic gas plume CO_2/SO_2 ratio. Journal of Volcanology and Geothermal Research, 182, 221-230.

Aiuppa, A., Moretti, R., Federico, C., Giudice, G., Gurrieri, S., Liuzzo, M., Papale, P., Shinohara, H., Valenza, M., (2007) Forecasting Etna eruptions by real-time observation of volcanic gas composition. Geology, 35, 1115-1118.

Aiuppa, A., Bagnato, E., Witt, M. L. I., Mather, T. A., Parello, F., Pyle, D. M., Martin, R. S. (2007) Real-time simultaneous detection of volcanic Hg and SO_2 at La Fossa Crater, Vulvano (Aeolian Islands, Sicily). Geophysical Research Letters, 34, L21307.

Aiuppa, A., (2009) Degassing of halogens from basaltic volcanism: insights from volcanic gas observations. Chemical Geology, 263, 99-109.

Aiuppa, A., Baker, D. R., Webster, J. D. (2009) Halogens in volcanic systems. Chemical Geology, 263, 1-18.

Allard, P., Aiuppa, A., Loyer, H., Carrot, F., Gaudry, A., Pinte, G., Michel, A., Dongarra, G., (2000) Acid Gas and metal Emission Rates during Long-lived Basalt Degassing at Stromboli Volcano. Geophysical Research Letters 27, 1207-1210.

Alletti, M., Baker, D.R., Freda, C. (2006) Halogen diffusion in basaltic melt. Geophysical Research Abstracts, 8, 05936.

Alleti, M., Aiuppa, A., Baker, D. R., Freda, C. (2006) Fluid/melt partitioning coefficients of chlorine in basaltic melt. Geophsical Research Abstracts, 8(08823).

Alletti, M., Baker, D.R., Freda, C., (2007) Halogen diffusion in basaltic melt. Geochimica et Cosmochimica Acta, 71, 3570-3580.

Aletti, M., Baker, D.R., Scaillet, B., Aiuppa, A., Moretti, R., Ottolini, L (2009) Chlorine partitioning between a basaltic melt and H2O-CO2 fluids at Mount Etna. Chemical Geology, 263, 37-50.

Andres, R. J., Kyle, P. R., Chuan, R. L. Sulphur dioxide, particle and elemental emissions from Mount Etna, Italy during July 1987. Geology Rundsh, 82, 687-95.

Baker, L., Rutherford, M.J., (1996) Sulfur diffusion in rhyolite melts. Contributions to Mineralogy and Petrology, 123, 335–344.

Baker, L., Rehkamper, M., Hinkley, T. K., Nielsen, S. G., Toutain, J. P. (2009) Investigation of thallium fluxes from subaerial volcanism – Implications for the present and past mass balance of thallium in the oceans. Geochimica et Cosmochimica Acta, 73, 6340-59.

Balcone-Boissard, H., Baker, D. R. Villemant, B., Bouden, G. (2009) F and Cl diffusion in phonolitic melts: influence of the Na/K ratio. Chemical Geology, 263, 89-98.

Carroll, M.R., Holloway, J.R., (Eds) (1994) Volatiles in Magmas: Reviews in Mineralogy. Vol 30. Washington, DC, Mineralogical Society of America.

Chakraborty, S. (1995) Diffusion in silicate melts. In Structure, Dynamics and Properties of Silicate Melts, Mineralogical Society of America (eds. Stebbins J.F., McMillan P.F., Dingwell D.B.) 32, 411-497.

Churakov S. V., Tkachenk, S.I., Korzhinskii, M.A., Bocharnikov, R.E., Shmulovich, K.I. (2000) Evolution of Composition of High-Temperature Fumoralic Gases from Kudryavy Volcano, Iturup, Kuril Islands: the Thermodynamic Modeling. Geochemisry International, 28(5), 436-51.

Cioni R., Sulpizio, R., Garruccio N (2003) Variability of the eruption dynamics during a Subplinian event: the Greenish Pumice eruption of Somma-Vesuvius (Italy). Journal of volcanology and geothermal research. 124, 89-114

Clausen, O., Russel, C. (1997) Thermodynamics of various polyvalent main group elements in a borosilicate glass melt. Journal of non-crystalline solids, 209, 292-98.

Clausen, O., Russel, C. (1997) Self diffusion of polyvalent ions in a borosilicate glass melt. Journal of non-crystalline solids, 215, 68-74.

Clausen, O., Gerlach, S., Russel, C. (1999) Self-diffusivity of polyvalent ions in silicate liquids. Journal of non-crystalline solids, 253, 76-83.

Crank, J. (1975) The Mathematics of Diffusion. 2nd ed., Oxford University Press, 11-43.

Crowe, B.M., Finnegan, D.L., Zoller, W.H., Boynton, W. (1987) Trace Element Geochemistry of Volcanic Gases and Particles From 1983-1984 Eruptive Episodes of Kilauea Volcano. Journal of Geophysical Research, 92, 13708-13714.

Delaney, J.R., Karsten, J.L., Ion microprobe studies of water in silicate melts. Concentration-dependent water diffusion in obsidian, Earth and Planetary Science Letters, 52, 191–202.

Dingwell, D. B., Scarfe, C. M. (1985) Chemical diffusion of fluorine in melts in the system Na2O-Al2O3-SiO2. Earth and Planetary Science Letters, 73, 377-384.

Epstein, P. S., Plesset, M.S. (1950) On the stability of gas bubbles in liquid-gas solutions. The Journal of Chemical Physics, 18(11), 1505-09.

Ertel, W., Dingwell, D.B., Sylvester P. J., (2006) Siderophile elements in silicate melts – A review of the mechanically assistes equilibrium technique and the nanonugget issue. Chemical geology, 248, 119-139.

Ferrara, R., Mazzolai, B., Lanaillotta, E., Nucaro, E., Pirrone, N. (2000) Volcanoes as emission sources of atmospheric mercury in the Mediterranean basin. The Science of the Total Environment, 259, 115-121.

Freda, C., Baker, D.R., Scarlato, P., (2005) Sulfur diffusion in basaltic melts. Geochimica et Cosmochimica Acta, 69, 5061–5069.

Freer, R. (1981) Diffusion in silicate minerals and glasses: a data digest and guide to the literature. Contribution to Mineralogy and Petrology, 76, 440-54.

Friele P.A., Clague, J.J. (2004) Large Holocene landslides from Pylon Peak, southwestern British Columbia. Canadian Journal of Earth Science, 41, 165–182.

Gardner, J. E., Hilton, M., Carroll, M. R. (1999) Experimental constrains on degassing of magma: isothermal bubble growth during continuous decompression from high pressure.Earth and Planetary Science Letters, 168, 201-18.

Gauthier, P. J, Le Cloarec, M. F. (1998) Variability of alkali and heavy metal fluxes released by Mt. Etna volcano, Sicily, between 1991 and 1995. Journal of Volcanology and geothermal research, 81, 311-26.

Gerlach, S., Clausen, O., Russel, C. (1998) Self-diffusivity of iron in alkali-lime-aluminosilicate glass melts. Journal of non-crystalline solids, 240, 110-17.

Gemmell, J. B. (1987) Geochemistry of metallic trace elements in fumarolic condensates from Nicaraguan and Costa Rican volcanoes. Journal of Volcanology and Geothermal Research, 33, 161-181.

Giggenbach, W. F. (1975) Variations in the Carbon, Sulfur and Chlorine contents of Volcanic Gas Discharges from White Island, New Zealand. Bulletin of Volcanology, 43(3) 253-255.

Gustin, M. S., Lindberg, S. E. (2000) Assessing the contribution of natural sources to the global mercury cycle: The importance of intercomparing dynamic flux measurements. Fresenius J Anal Chem, 366, 417-22.

Gustin, M. S., Lindberg, S. E., Weisberg, P. J. (2008) An update on the natural sources and sinks of atmospheric mercury. Applied Geochemistry, 23, 482-493.

Hedenquist, J. W. (2004) The ascent of magmatic fluid: discharge versus mineralization. MAC short course series: 263-289.

Henderson, P., Nolan, J. Cunningham, G. C., Lowry, R. K. (1985) Structural controls and mechanisms of diffusion in natural silicate melts. Contributions to Mineralogy and Petrology, 89, 263-72.

Hinkley, T.K., Le Cloarec, M.-F., Lambert, G. (1994) Fractionation of families of major, minor, and trace metals across the melt-vapor interface in volcanic exhalations. Geochimica et Cosmochimica Acta, 58, 3255-3263.

Hinkley, T. K., Lamothe, P. J., Wilson, S. A., Finnegan, D. L., Gerlach, T. M. (1999) Metal emissions from Kilauea, and a suggested revision of the estimated worldwide metal output by quiescent degassing of volcanoes. Earth and Planetary Science Letters, 170, 315-325.

Hirabayashi, J., Ossaka, J., Ozawa, T. (1982) Relationship between volcanic activity and chemical composition of volcanic gases – A case study on the Sakurajima Volcano. Geochemical Journal, 16, 11-21.

Hofmann, A.W. (1980). Diffusion in natural silicate melts: A critical review. In Physics of magmatic processes (Hargraves, R. B., ed.). Princeton University Press, 385-417.

Jambon, A. (1982) Tracer Diffusion in granitic melts: Experimental results of Na, K, Rb, Cs, Ca, Sr, Ba, Ce Eu, To at 1300 °C and a model calculation. Journal of Geophysical Research, 87(B13), 10,797-10,810.

Jugo, P., Luth, R., Richards, J.P. (2005) An Experimental Study of the Sulfur Content in Basaltic Melts Saturated with Immiscible Sulfide or Sulfate Liquids at 1300 °C and 1.0 GPa. Journal of Petrology, 46(4), 783-798.

Kretz, R. (1994) Metamorphic Crystallization. John Wiley & Sons. New York, NY. 276-291.

Lyakhovsky, V., Hurwitz, S., Navon, O. (1996) Bubble growth in rhyolitic melts: experimental and numerical investigation. Bulletin of Volcanology, 58, 19-32.

MacKenzie, J.M., Canil, D. (2006) Experimental constraints on the mobility of Rhenium in silicate liquids. Geochimica et Cosmochimica Acta, 70, 5236-5245.

MacKenzie, J.M., Canil, D. (2008) Volatile heavy metal mobility in silicate liquids: Implications for volcanic degassing and eruption prediction. Earth and Planetary Science Letters, 269, 488-496.

Mackenzie, J.M., Canil, D. (in press) Fluid/melt partitioning of Re, Mo, W, Tl and Pb in the system haplobasalt-H_2O-Cl and the volcanic degassing of trace metals.

Menyailov, I. A. (1975) Prediction of Eruptions using changes in composition of volcanic gases. Bulletin of Volcanology. 39, 112-125.

Menyailov, I. A., Nikitina, L. P., Shapar, V. N., Pilipenko, V. P. (1986) Temperature increase and chemical change of fumarolic gases at Momotombo volcano, Nicaragua, in 1982-1985: Are these indicators of a possible eruption? Journal of Geophysical Research Letters, 91(B12), 12199-214.

Michol, K.A., Russell, J.K., Andrews, G.D.M. (2008) Welded block and ash flow deposits from Mount Meager, British Columbia, Canada. Journal of Volcanology and Geothermal Research 169, 121–144.

Moriizumi M., Nakashima, S., Okumura, S., Yamonai, Y. (2009) Color-change processes of a plinian pumice and experimental constraints of color-change kinetics in air of an obsidian. Volcanology Bulletin, 71, 1-13.

Mungall, J. E., Dingwell, D. B. (1997) Actinide diffusion in a haplogranitic melt: Effects of temperature, water content, and pressure. Geochimica et Cosmochimica Acts, 61(11), 2237-46.

Mungall, J. E., Dingwell, D. B., Chaussidon, M. (1999) Chemical diffusivities of 18 trace elements in granitoid melts. Geochimica et Cosmochimica Acts, 63(17), 2599-2610.

Ni, H., Behrens, H., Zhang Y. (2009) Water diffusion in dacitic melt. Geochimica et Cosmochimica Acta 73, 3642–3655

Noguchi, K., Kamiya, H. (1963) Prediction of volcanic eruption by measuring the chemical composition and amounts of gases. Bulletin of Volcanology, 26, 367-378.

Nowak, M., Schreen, D., Spickenbom, K. (2004) Ar and CO_2 on the race track in silicate melts: a tool for the development of a CO2 speciation and diffusion model. Geochimica et Comoschimica Acta, 68: 5127-5138.

Nriagu, J., (1989) A global assessment of natural sources of atmospheric trace metals. Nature, 338, 47-49.

Nriagu, J., Becker, C. (2003) Volcanic emissions of mercury to the atmosphere: global and regional inventories. The Science of the Total Environment, 304, 3-12.

Ohba, T., Hirabayashi, J., Nogami, K., Kusakabe, M., Yoshida, M. (2008) Magma degassing process during the eruption of Mt. Unzen, Japan in 1991 to 1995: Modeling with the chemical composition of volcanic gas. Journal of Volcanology and Geothermal Research, 175, 120-132.

Olmez, I., Finnegan, D. L., Zoller, W. H. (1986) Iridium emissions from Kilauea Volcano. Journal of Geophysical Research, 91, 653-63.

Orsi, G., Gallo, G., Heiken G., Wohletz, K., Yu, E., Bonani, G. (1992) A comprehensive study of pumice formation and dispersal: the Cretaio Tephra of Ischia (Italy). Journal of Volcanology and Geothermal Research, 53, 329-354.

Pennisi, M., Le Cloarec, M.F., Lambert, G., Le Roulley, J.C. (1988) Fractionation of metals in volcanic emissions. Earth and Planetary Science Letters, 88, 284-288.

Peregoedova, A., Barnes, S. J., Baker, D. R. (2006) An experimental study of mass transfer of platinum-group elements, gold, nickel and copper in sulfur-dominated vapor at magmatic temperatures. Chemical Geology, 235, 59-75.

Perez, W. A., Dunn, T. (1996) Diffusivity of strontium, neodymium, and lead in natural rhyolite melt at 1.0 Gpa. Geochimica et Cosmochimica Acta, 60, 1387-97.

Proussevitch, A. A., Sahagian, D. L., Kutolin, V. A. (1993) Stability of foams in silicate melts. Journal of Volcanology and Geothermal Research, 59, 161-78.

Pyle, D. M., Mather, T. A. (2003) The importance of volcanic emissions for the global atmospheric mercury cycle. Atmospheric Environment, 37, 5115-24.

Rubin, K. (1997) Degassing of metals and metalloids from erupting seamount and mid-ocean ridge volcanoes: Observations and predictions. Geochimica et Cosmochimica Acta, 61, 3525-3542.

Russell, J. K., Hickson, C. J., Andrews, G. (2007) Canadian Cascade volcanism: Subglacial to explosive eruptions along the Sea to Sky Corridor, BC. Geological Society of America field guide, 9, 1-29.

Rust, A. C., Russell, J. K., Knight, R. J. (1999) Dielectric constand as a predictor of porosity in dry volcanic rocks. Journal of Volcanology and Geothermal Research. 91, 79-96.

Self, S., Blake, S., Sharma, K.,Widdowson, Sephton, S. (2008) Sulfur and Chlorine in Late Cretaceous Deccan Magmas and Eruptive Gas Release. Science 319, 1654-56.

Shane, P., Froggatt P., Smith, I., Gregory, M. (1988) Multiple Sources for Sea-Rafted Loisels Pumice, New Zealand. Quaternary Research, 49**,** 271–279

Shaw, R. P. (1974) An integral equation approach to diffusion. Journal of Heat Mass Transfer, 17, 693-99.

Shelby, J.E. (2005) Introduction to Glass Science and Technology 2nd Edition. Royal Society of Chemistry. Cambridge, UK.

Shinohara, H., (2008) Excess degassing from volcanoes and its role on eruptive and intrusive activity. Review of Geophysics, 46(RG4005).

Shinohara, H., Aiuppa, A., Giudice, G., Gurrieri, S., Liuzzo, M. (2008) Variation of H_2O/CO_2 and CO_2/SO_2 ratios of volcanic gases discharged by continuous degassing of Mount Etna volcano, Italy. Journal of Geophysical Research, 113(B09203).

Signorelli, S. (1997) Arsenic in volcanic gasses. Environmental Geology, 32, 239-43.

Simon, A. C., Pettke, T., Candela, P. A., Piccoli, P. M., Heinrich, C. A. (2007) The partitioning behavior of As and Au in S-free and S-bearing magmatic assemblages. Geochimica et Cosmochimica Acta, 71, 1764-82.

Smith, V.G., Tiller, W.A., Rutter, J.W. (1955) A mathematical analysis of solute redistribution during solidification. Canadian Journal of Physics, 33, 723–744.

Sparks, R.S.J. (1978) The dynamicsof bubble formation and growth in magmas: a review and analysis. Journal of Volcanology and Geothermal Research, 3, 1-37.

Tait, S., Thomas, R., Gardner, J., Jaupart, C. (1998) Constraints on cooling rates and permeabilities of pumice in an explosive eruption jet from colour and magnetic mineralogy. Journal of Volcanology and Geothermal Research 86, 79–91.

Taran, Y., Gavilanes, J. C., Cortes, A. (2002) Chemical and isotopic composition of fumarolic gases and the SO2 flux from Vulcan de Colima, Mexico, between the 1994 and 1998 eruptions. Journal of Volcanology and Geothermal Research, 117, 105-119.

Tuzzolo, M. R., Shelby, J. E. (1992) Hydrogen-induced formation of colloids of arsenic, antimony and bismuth in oxide glasses. Journal of non-crystalline solids, 143, 181-190.

Varekamp, J. C., Buseck, P. R. (1986) Global mercury flux from volcanic and geothermal sources. Applied Geochemistry, 1, 65-73.

Verhoogan, J. (1951) Mechanics of ash formation. American Journal of Science, 249, 729-739.

Villemant, B., Boudon, G. (1999) H2O and halogen (F, Cl, Br) behavior during shallow magma degassing processes. Earth and Planetary Science Letters, 168, 271-286.

Wallace, P.J. (2005) Volatiles in subduction zone magmas: concentrations and fluxes based on melt inclusion and volcanic gas data. Journal of Volcanology and Geothermal Research, 140, 217-240.

Wardell, L. J., Kyle, P. R., Counce, D. (2008) Volcanic emissions of metals and halogens from White Island (NZ) and Erebus volcano (Antarctica) determined with chemical traps. Journal of Volcanology and Geothermal Research, 177, 734-42.

von der Gonna, G., Russel, C. (2000) Diffusivity of various polyvalent elements in a Na_20-SiO_2 glass melt. Journal of non-crystalline solids, 261, 204-210.

Watson, E.B., Sneeringer, M.A., Ross, A. (1982) Diffusion of dissolved carbonate in magmas: experimental results and applications. Earth and Planetary Science Letters, 61, 346–358.

Watson (1994) Diffusion in volatile-bearing magmas. In Reviews in Mineralogy (Carroll, M.R., Holloway, J.R., eds.) Vol 30, 372-411.

Yudovskaya, M.A., Tessalina, S., Distler, V.V., Chaplygin, I.V., Chugaev, A.V., Dikov, Y.P. (2008) Behavior of highly-siderophile elements during magma degassing: A case study at the Kudryavy volcano. Chemical Geology, 248, 318-341.

Zreda-Gostynska G, Kyle PR (1997) Volcanic gas emissions from Mount Erubus and their impact on the Antarctic environment. J. Geophys. R. 102(B7): 15,039-55.

APPENDIX I: Arrhenius Plots

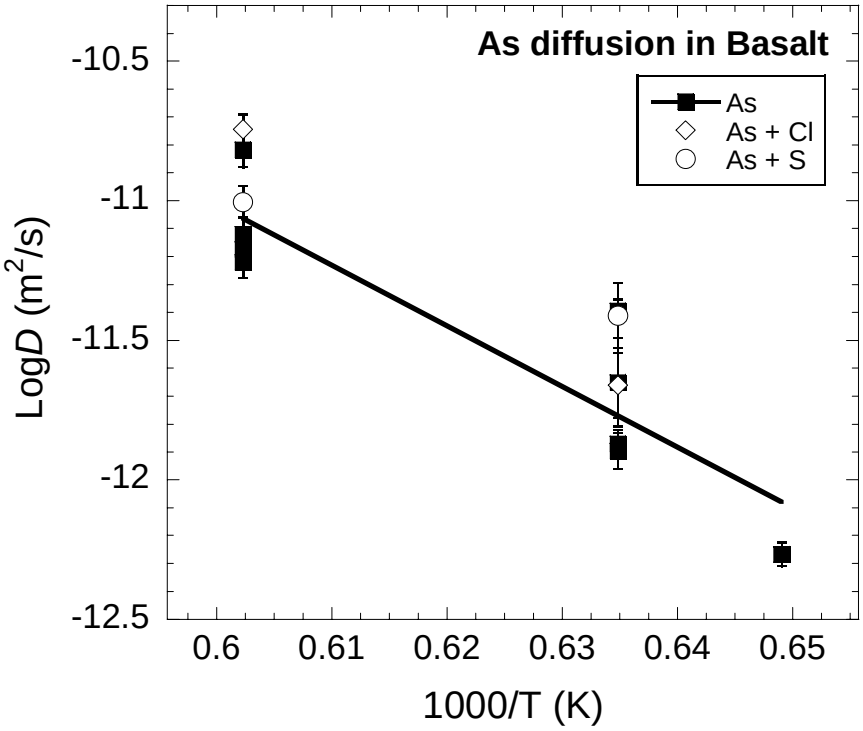

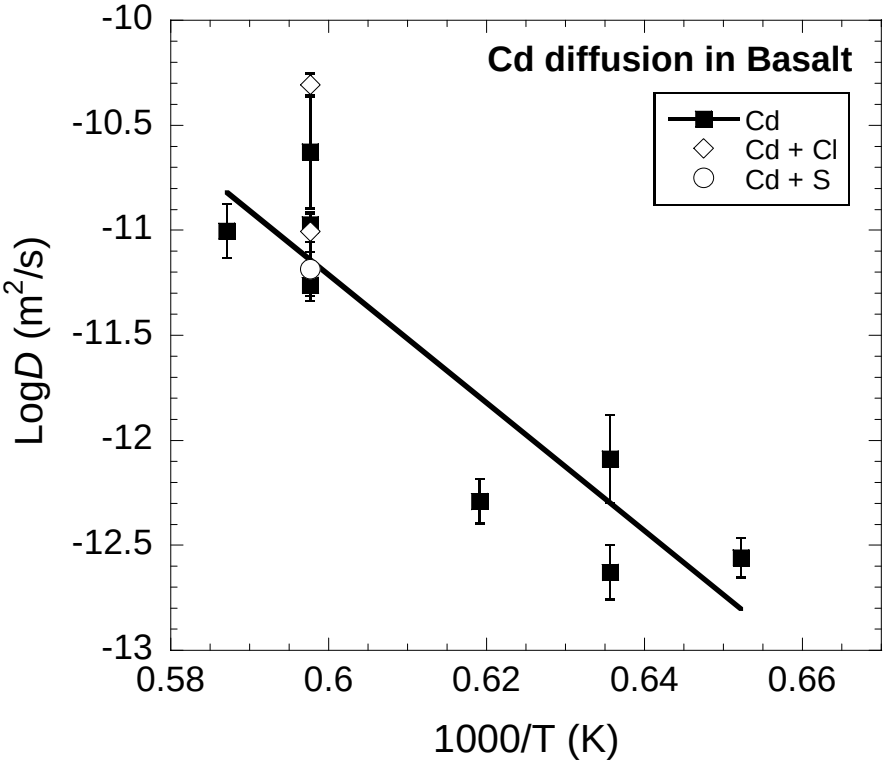

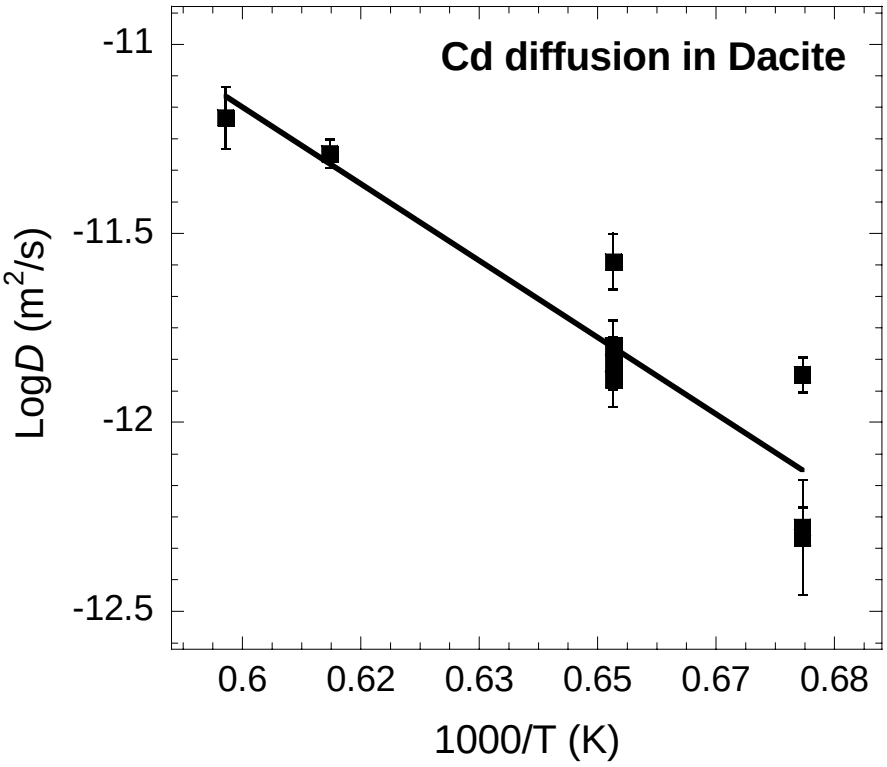
Cd diffusion in Dacite
-11
-11.5
-12
-12.5
Log$D$ (m^2/s)
0.6
0.62
0.63
0.65
0.67
0.68
1000/T (K)

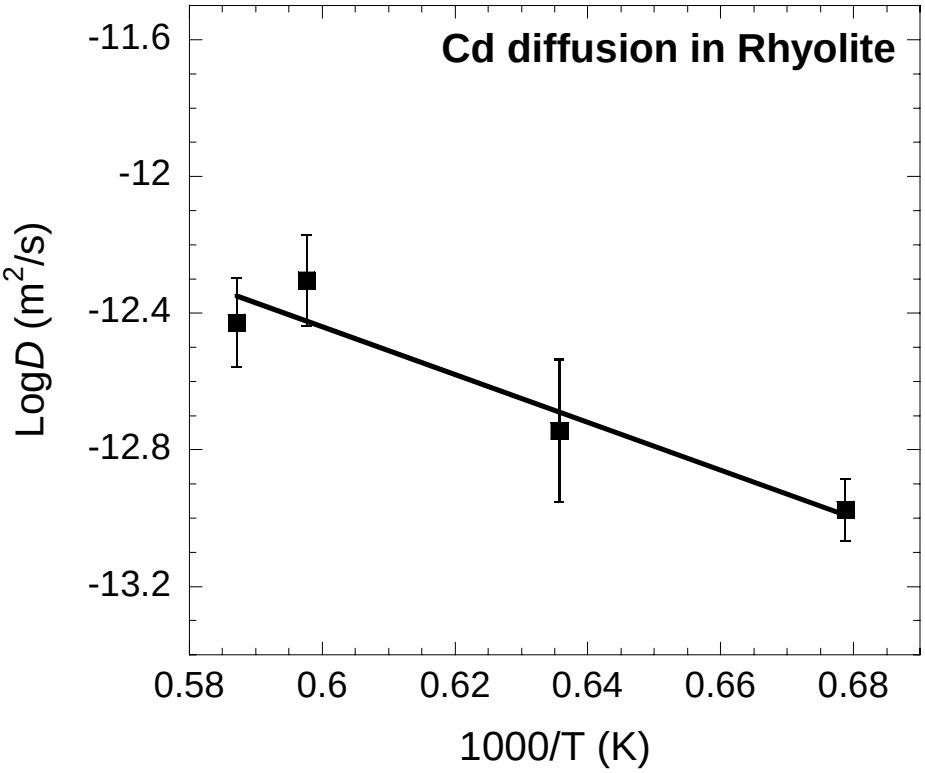
Cd diffusion in Rhyolite
-11.6
-12
-12.4
-12.8
-13.2
Log$D$ (m^2/s)
0.58
0.6
0.62
0.64
0.66
0.68
1000/T (K)

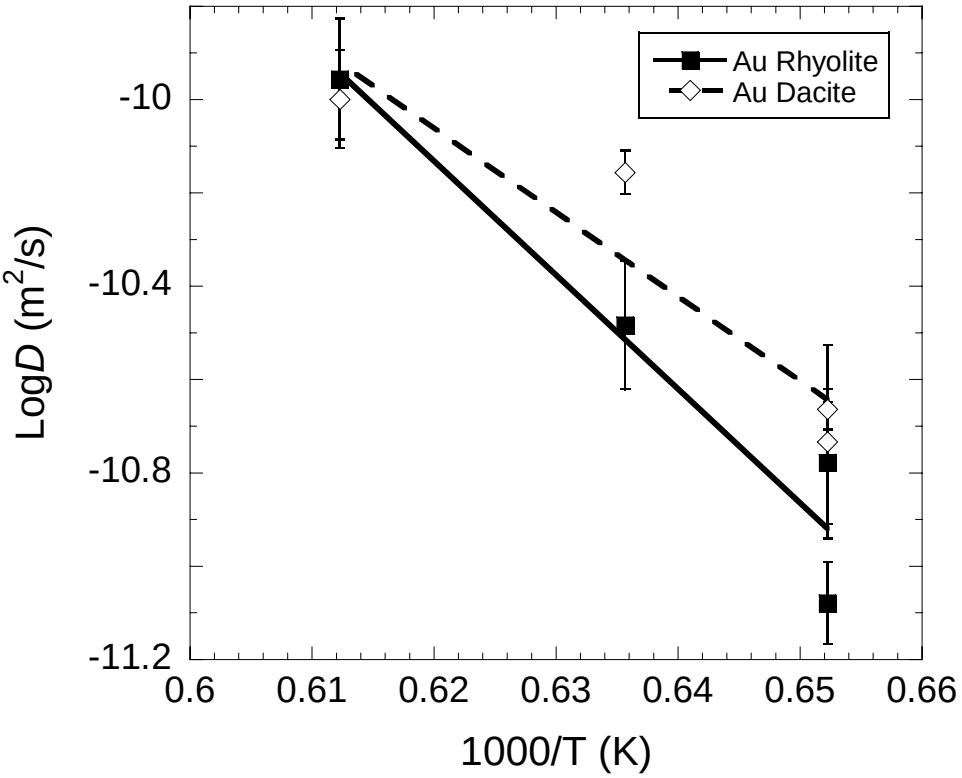
Au Rhyolite
Au Dacite
-10
-10.4
-10.8
-11.2
Log$D$ (m^2/s)
0.6
0.61
0.62
0.63
0.64
0.65
0.66
1000/T (K)

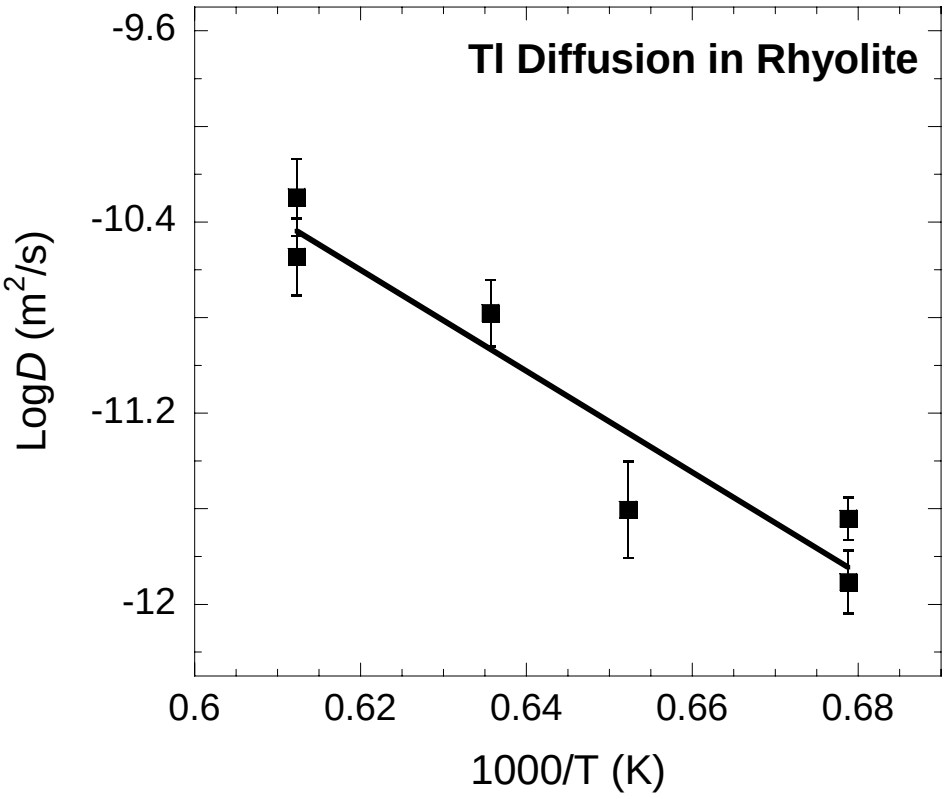
Tl Diffusion in Rhyolite
-9.6
-10.4
-11.2
-12
Log$D$ (m^2/s)
0.6
0.62
0.64
0.66
0.68
1000/T (K)

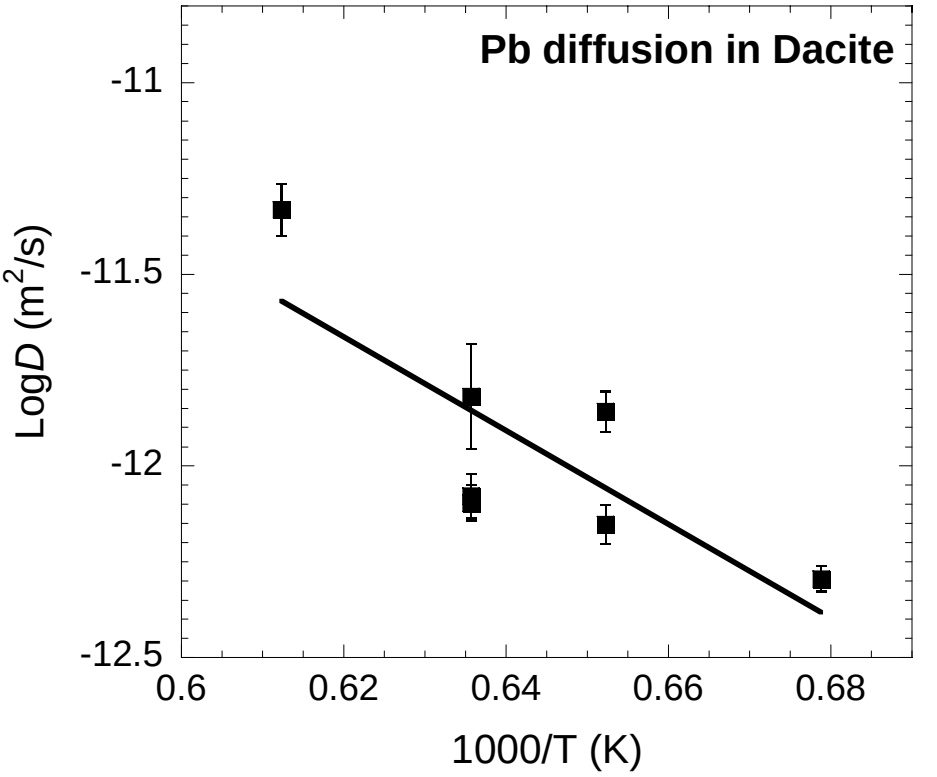
Pb diffusion in Dacite
-11
-11.5
-12
-12.5
Log$D$ (m^2/s)
0.6
0.62
0.64
0.66
0.68
1000/T (K)

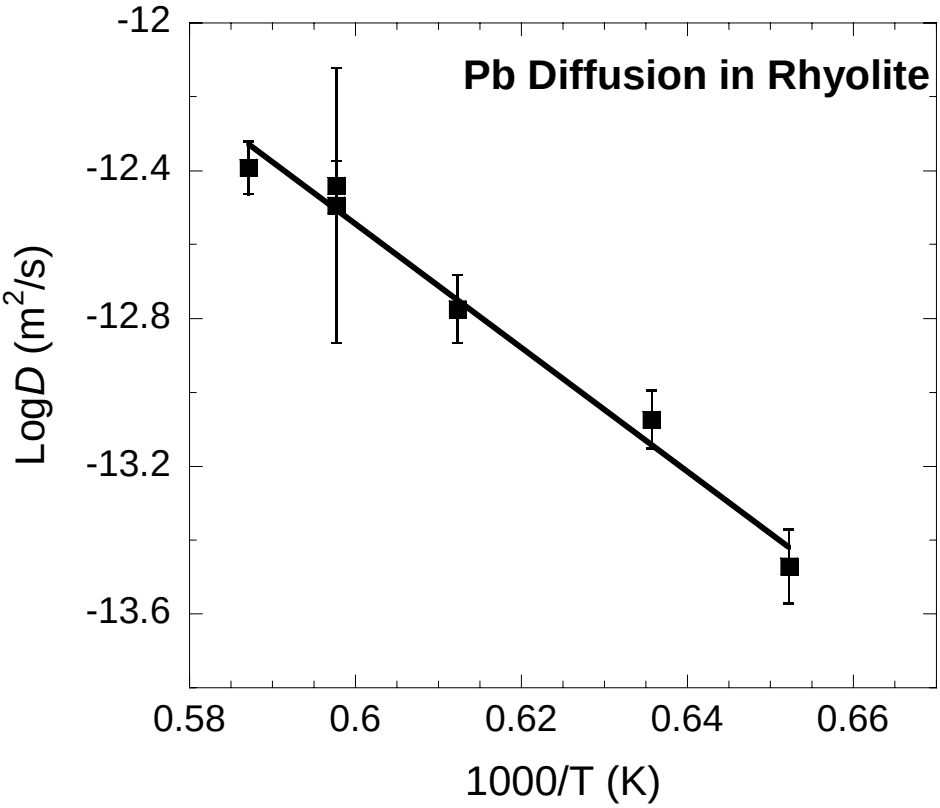
Pb Diffusion in Rhyolite
-12
-12.4
-12.8
-13.2
-13.6
Log$D$ (m^2/s)
0.58
0.6
0.62
0.64
0.66
1000/T (K)

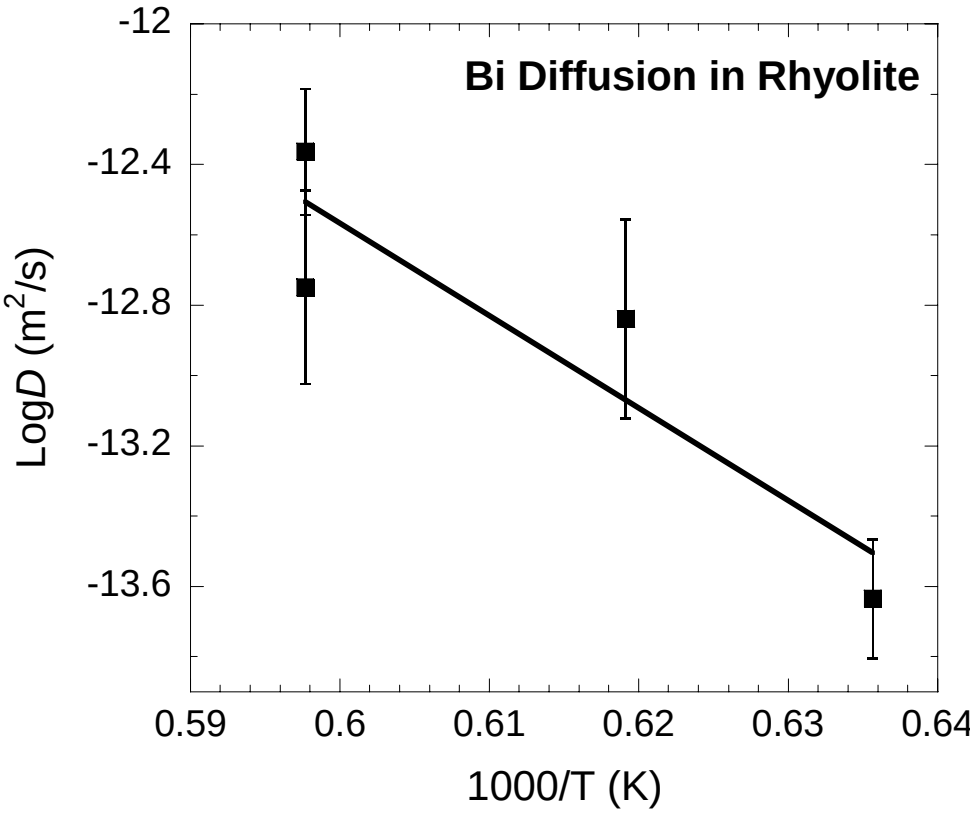
Bi Diffusion in Rhyolite
-12
-12.4
-12.8
-13.2
-13.6
Log$D$ (m^2/s)
0.59
0.6
0.61
0.62
0.63
0.64
1000/T (K)